Geochemistry, Geophysics, Geosystems®

RESEARCH ARTICLE
10.1029/2022GC010452

Key Points:

- Chemical signatures in the deep waters of the southern Central Indian Ridge, at 24°49'S, provide evidence for hydrothermal plumes
- Enrichment of volatiles (helium and methane) over metals (manganese and iron) in plumes indicate the influence of ultramafic rocks
- Presence of sulfide and sulfate particles (pyrite, chalcopyrite and barite) in plumes may indicate the high-temperature venting in the vicinity

Correspondence to:
P. John Kurian,
john@ncpor.res.in

Citation:
Surya Prakash, L., John Kurian, P., Resing, J. A., Tsunogai, U., Srinivas Rao, A., Sen, K., et al. (2022). Volatile-rich hydrothermal plumes over the southern Central Indian Ridge, 24°49'S: Evidence for a new hydrothermal field hosted by ultramafic rocks. *Geochemistry, Geophysics, Geosystems*, *23*, e2022GC010452. https://doi.org/10.1029/2022GC010452

Received 25 MAR 2022
Accepted 7 JUL 2022

Author Contributions:

Conceptualization: L. Surya Prakash, P. John Kurian
Data curation: L. Surya Prakash
Formal analysis: L. Surya Prakash, J. A. Resing, U. Tsunogai, K. Sen
Funding acquisition: P. John Kurian
Investigation: L. Surya Prakash, A. Srinivas Rao, K. Sen, A. Prajith
Methodology: L. Surya Prakash, P. Roy
Project Administration: P. John Kurian
Resources: J. A. Resing, U. Tsunogai, J. E. Lupton, P. Roy
Supervision: P. John Kurian

Volatile-Rich Hydrothermal Plumes Over the Southern Central Indian Ridge, 24°49'S: Evidence for a New Hydrothermal Field Hosted by Ultramafic Rocks

L. Surya Prakash[1], P. John Kurian[1], J. A. Resing[2], U. Tsunogai[3], A. Srinivas Rao[1], K. Sen[1], J. E. Lupton[4], T. Baumberger[4,5], A. Prajith[1], and P. Roy[1]

[1]National Centre for Polar and Ocean Research, Ministry of Earth Sciences, Vasco-da-Gama, India, [2]Cooperative Institute for Climate, Oceans and Ecosystem Studies-University of Washington, and NOAA-PMEL, Seattle, WA, USA, [3]Graduate School of Environmental Studies, Nagoya University, Nagoya, Japan, [4]Cooperative Institute of Marine Resources Studies Oregon State University, Newport, OR, USA, [5]NOAA Pacific-Marine Environmental Laboratory, Newport, OR, USA

Abstract Water column physico-chemical studies were conducted over the southern Central Indian Ridge between 24°44'S and 25°52'S to identify and chemically characterize seafloor hydrothermal activity. High turbidity values were observed between 2300 and 2700 m with two distinct layers, between water depths of 2320–2500 m and 2510–2650 m, at two closely spaced CTD stations at 24°48.62'S (CTD-17-P5) and 24°48.68'S (CTD-17-P8). Elevated concentrations of dissolved Mn (DMn: 19–112 nM), dissolved Fe (DFe: 33–88 nM), methane (CH_4: 32–246 nM), elevated δ^3He values (28%–88%), and stable carbon isotope ratios of CH_4 confirm the hydrothermal origin. In plume layer-1, the maximum concentrations were observed at 2375m at P8 and in plume layer-2, the maximum concentrations were observed at 2570 m at P5. The stable isotope ratios of methane (δ^{13}C-CH_4) show that heavier isotopes are enriched (−13.2‰ to −14.7‰) in the plume waters and are similar to vent fluids on the global mid-oceanic ridges. Further, morphological and mineralogical studies of plume particles, collected from the plume layer-2 maxima, clearly show the presence of barite, pyrite, chalcopyrite, and indicate possible venting of high-temperature fluids in the vicinity of P5. Enrichment in methane relative to the other tracers and the general geochemical characteristics of these two plume layers, CH_4/Mn (1.8–2.2); CH_4/Δ^3He (85–97 × 10^6), Mn/Δ^3He (44–46 × 10^6), Fe/Δ^3He (52–54 × 10^6), indicate that these plumes are formed from fluids released at the seafloor that circulated through ultramafic/gabbroic rocks. The high concentrations of dissolved gases and metals combined with the presence of sulfide particles in the water column provide evidence for a new ultramafic/gabbroic-hosted hydrothermal vent field, at 24°49'S on the southern Central Indian Ridge.

Plain Language Summary Evidence for the seafloor hydrothermal activity was first discovered in 1970. Since then, numerous vent fields were discovered in Atlantic, Indian and Pacific Oceans. Among these three oceans, Indian Ocean is relatively less explored and most of the hydrothermal fields were discovered along the Central Indian Ridge. A multi-disciplinary team, expertise in geophysics, geology, physical, chemical and biological oceanographers, has to work together to discover these fields. Extensive water column studies have been carried out on the southern Central Indian Ridge to identify plumes. High concentrations of manganese, iron, methane, and helium values between 2300 and 2700 m confirm the presence of hydrothermal plumes. The nature of the particles collected from these plumes shows that most of them are sulfides, sulfate and oxides of iron. The geochemical ratios in these plumes (combination of gas/metal and metal/gas) show that the fluid composition is controlled by ultramafic rocks. The chemical composition of both fluid and plume is mainly controlled by the rock type (basalt and/or ultramafic) of the sub-seafloor. The high concentrations of gases and metals in the water column provide evidence for a new hydrothermal vent field, at 24°49'S on the southern Central Indian Ridge.

1. Introduction

The Central Indian Ridge (CIR) has been better explored for hydrothermal plumes in the water-column compared to the other parts of the Indian mid-oceanic ridge system such as the Carlsberg, Southeast, and Southwest Indian Ridges. Numerous studies have focused on identification of hydrothermal plume signatures in the water column and ultimately led to the discovery of vent fields (Gamo et al., 1996; Jean-Baptiste et al., 1992; Kawagucci

Validation: L. Surya Prakash, A. Srinivas Rao, K. Sen
Writing – original draft: L. Surya Prakash
Writing – review & editing: P. John Kurian, J. A. Resing, U. Tsunogai, J. E. Lupton, T. Baumberger

et al., 2008; Nakamura et al., 2012; Ray et al., 2020; Son et al., 2014; You et al., 2014). In continuation of these studies, hydrothermal vent fields have been discovered at eight different sites, between 8° and 27°S, ranging from basaltic to ultramafic hosted systems (Gamo et al., 2001; Kawagucci et al., 2008, 2016; Kim et al., 2020; Nakamura et al., 2012; Ryu et al., 2019; Van Dover et al., 2001). In the year 2000, the first active hydrothermal site, the Kairei vent field (Gamo et al., 2001), was discovered in the Indian Ocean at the southernmost end of the CIR (at 25°19'S), with the other sites being discovered thereafter. Of the eight known active hydrothermal fields along the CIR, four are located along the northern CIR (8°–12°S), and four (Kairei, Edmond, Solitaire, and Dodo) in the southern CIR (18°–27°S).

Along the northern CIR, Onnuri hydrothermal vent field, located (11°24.9'S; 66°25.4'E), was the first reported site of hydrothermal activity (Ryu et al., 2019). Subsequently, three more hydrothermal fields were also discovered at 8°10.1'S, 9°47.5'S, and 9°48.9'S (Kim et al., 2020). Along the southern CIR, four vent fields, Kairei (25°19'S), Edmond (23°52'S), Solitaire (19°33'S), and Dodo (18°20'S), have been discovered (Gamo et al., 2001; Kawagucci et al., 2008, 2016; Nakamura et al., 2012; Van Dover et al., 2001). Among the eight vent fields found along the CIR, mantle-derived peridotites and gabbros have been recovered from Kairei, Onnuri and 8°10.1'S vent fields, and venting at these sites was consistent with ultramafic hosted hydrothermal systems (Kawagucci et al., 2016; Kim et al., 2020; Kumagai et al., 2008). The spreading rate and presence of mantle-derived rocks along the CIR is very similar to the slow-spreading Mid-Atlantic Ridge (MAR). The spreading rate of the MAR is less than 40 mm/yr and diverse types of ultramafic hosted hydrothermal systems such as Rainbow, Logatchev and Lost City are present (Charlou et al., 2002; Kelley et al., 2005). The Dodo field is located at the center of the axial valley floor, where large-scale basaltic sheet-flow lava is observed, likely due to excess melt supply. The Solitaire field is located slightly away from the neo-volcanic zone in an area where a MOR neo-volcanic zone intersects with intra-plate volcanism (Kawagucci et al., 2016). The Edmond and Kairei fields are located on the axial valley wall at the northern end of segments S3 and S1 (as defined by Briais, 1995). However, the Kairei field is characterized by the presence of gabbro and perodotite rocks.

The geochemical composition of Dodo, Solitaire, Edmond, and Kairei vent fluids have been well documented, and reflect the relationship between fluid chemistry and tectonic-geological environment (Gallant & Von Damm, 2006; Gamo et al., 2001; Kawagucci et al., 2016; Kumagai et al., 2008; Nakamura et al., 2012; Van Dover et al., 2001). The fluid chemistries of Solitaire, Edmond, and Dodo fields show characteristics of basalt-hosted hydrothermal systems (Gallant & Von Damm, 2006; Kawagucci et al., 2016) and are similar to basalt-hosted vent fields found elsewhere, including Trans-Atlantic Geotravers (TAG) and Snakepit on Mid-Atlantic ridge and 11°N, 13°N, 21°N on East Pacific Rise (Charlou et al., 1996, 2000). However, Soltaire has elevated $^{3}He/^{4}He$ ratio (8.96 relative to atmosphere) reflecting the impact of the Réunion hotspot mantle plume (Füri et al., 2011; Graham, 2002), while elevated hydrogen concentrations in the Dodo fluids are thought to be associated with neovolcanic activity (Kawagucci et al., 2016). Kairei vent fluids are characterized by very high hydrogen (up to 8 mM) and low methane (0.1–0.2 mM) concentrations due to serpentinization during seawater circulation through ultramafic mantle rocks (olivine-rich plutonic rocks with olivine gabbro-troctolite-dunite assemblages) and basalts (Kumagai et al., 2008; Nakamura et al., 2009; Takai et al., 2004). Kairei field is the only hydrothermal system in the Central Indian Ridge with this fluid chemistry which likely supports hyperthermophilic subsurface lithoautotrophic microbial ecosystem dominated by hyperthermophilic methanogens (Takai et al., 2004).

This study aims to explore and characterize new locations of seafloor hydrothermal activity along segment S2 of southern CIR (Briais, 1995). The ridge morphology and exposed rock type distribution of the study area (S2 of CIR) show characteristics of a typical slow-spreading ridge system, where gabbro and peridotite rocks are recovered from Kairei hydrothermal field and Yokoniwa Rise (Morishita et al., 2015; Nakamura et al., 2009). This unique type of geological setting provides an excellent opportunity to explore and characterize hydrothermal systems where the venting fluids probably may reflect both magmatic activity and circulation through ultramafic rocks. To accomplish these goals, we conducted geological and water column studies along the 50 km long segment S2. These studies map high turbidity signals in deep waters during repeated hydrocasts at several locations, consistent with the presence of hydrothermal activity. These data combined with hydrothermal plume chemistry (^{3}He, CH_4, Mn, and Fe) indicate that an undiscovered hydrothermal vent field must be present, representing the first report of seafloor hydrothermal activity over this segment.

2. Sampling and Analytical Methods

2.1. Geological Background

Three ridges, Central Indian Ridge (CIR), Southeast Indian Ridge (SEIR) and Southwest Indian Ridge (SWIR) in the Indian Ocean meet near 25°S (Figure 1a) to form a ridge-ridge-ridge type triple junction (Honsho et al., 1996) named the "Rodriguez Triple Junction". Here, the N-S trending CIR meets the NE-SW trending SWIR and

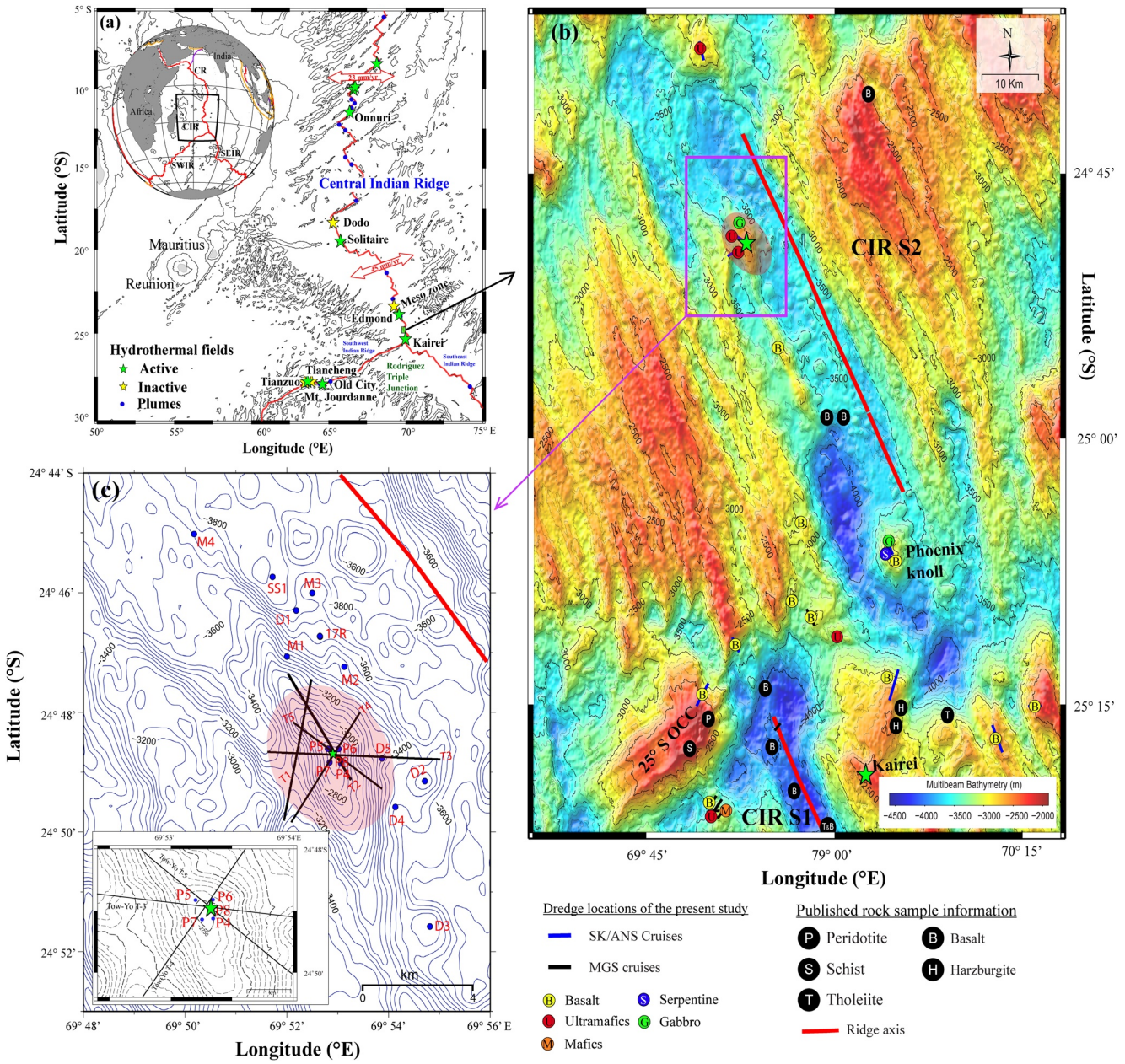

Figure 1. (a) Index map of Central Indian Ridge with hydrothermal vent fields (stars) and plumes (blue color circles). The information of vents and plumes is from Inter Ridge vents database. Thick red line represents the mid-oceanic ridge system in Indian Ocean and green and yellow stars represent the active and inactive vent fields. A small box filled with green color near Kairei field represents the present study area. (b) Bathymetry map of the Central Indian Ridge (CIR) segment S2 with major geological features (25°S OCC; Phoenix knoll at the southern end of the segment S2. Kairei field in the segment S1 is represented by green star. Geological sample types collected in the present study as well as published literature are shown with filled colored circles. Red colored transparent circle in the northern part of the segment S2 represents the present study area. (c) Bathymetry map of the present study area with vertical CTD stations (blue color circles) and tow-yo CTD tracks (black lines). Red colored transparent circle represents the region where water column anomalies were observed and green start represents the proposed location of the new hydrothermal field.

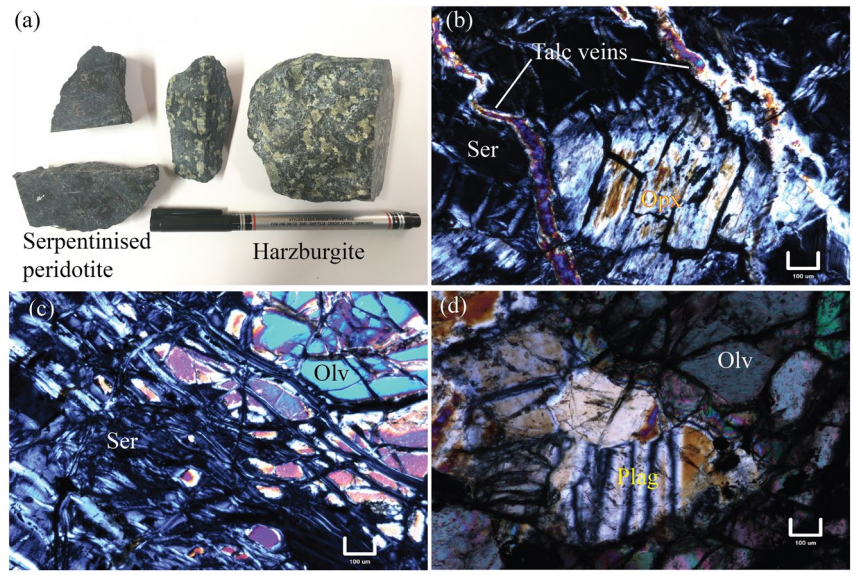

Figure 2. Macroscopic and microscopic view of rock samples from the study area. (a) Hand specimens of serpentinized peridotite and harzburgite (clasts of orthopyroxene are visible). (b) Harzburgite sample showing relict of orthopyroxene (Opx) set in a serpentinized matrix (Ser), crosscutting by talc veins. (c) Serpentinized peridotite (Ser) showing relicts of olivine (Olv) altered to serpentine. (d) Plagioclase (Plg) bearing peridotite showing presence of plagioclase feldspar surrounded by olivine (Olv).

NW-SE trending SEIR. It is interesting to note that the three ridges have different spreading rates and are classified as slow, ultraslow, and intermediate spreading ridges. The CIR is a slow to intermediate spreading ridge system with a full spreading rate that varies from 23 mm/yr at 10°S to 47 mm/yr at 25°S (DeMets et al., 2010; Kamesh Raju et al., 2012). The segmentation pattern of the southern CIR, from Rodriguez Triple Junction to 20°30'S, is given by Briais (1995), and the second segment (S2) shows many volcanic cones suggesting mantle upwelling in this region (Okino et al., 2015). On the southern end of the segment, typical oceanic core complexes (25°S) have formed on both sides of axial valley, and mantle-derived peridotites (fresh and altered type) have been recovered (Morishita et al., 2009; Okino et al., 2015; Sato et al., 2009). Petrological and geochemical studies of the Mid-Ocean Ridge Basalts (MORBs) collected from different parts of southern CIR (S1, S2 and S4) shows that melts were equilibrated with mantle olivine and indicate minor fractionation before the eruption (Sato et al., 2015).

The shallow axial depth and several volcanic cones around 24°50'S provide primary evidence for melt delivery (Okino et al., 2015). Dredge sampling was carried out by us on segment S2, recovered mantle-derived peridotites, plagioclase peridotite, and harzburgite from the dome-shaped axial high around 24°50'S and fresh basalts were recovered from the rift valley. Petrographic investigations of rock samples showed that the ultramafics are serpentinized with relicts of orthopyroxene, clinopyroxene, and olivine (Figure 2). In places, talc veins are present, crosscutting the serpentinized matrix (Figure 2), suggesting the latest stage of hydrothermal alteration. Previous studies (Morishita et al., 2015; Okino et al., 2015) also showed that ridge segments in the southern CIR hosts ultramafic rocks and are similar to other parts of northern CIR (Yi et al., 2014).

2.2. Water Sampling and Analytical Methods

During our cruise, onboard MGS Sagar (MGS-24), extensive water column surveys were carried out in the rift valley and around the axial highs of segment S2 to identify hydrothermal plume signatures. Both vertical hydro cast and tow-yo operations were conducted with a CTD-rosette package outfitted with Wetalabs optical backscatter sensor to identify particle-rich plumes. The turbidity anomaly (ΔNTU) was calculated by subtracting the background turbidity values from the maximum turbidity value in the plume layer. These operations were carried out at several locations covering both the rift valley and ridge flanks.

Seawater samples collected with 10 L Niskin sample bottles mounted on the CTD rosette and were sub-sampled for chemical tracers helium (^{3}He), manganese (DMn), iron (DFe), and methane (CH_4) and it's stable carbon isotopes (^{12}C and ^{13}C). Upon recovery of the CTD, samples for helium measurements were collected first, followed by methane, trace metals, and particulate matter. Detailed sample collection and analytical method for helium concentration and isotope studies are described by Lupton (1976, 1998). In brief, onboard, all seawater samples were collected in 1-foot copper tubing (in duplicates for each sample) and sealed by using a hydraulic crimper. At NOAA-PMEL in Newport, OR, USA, the dissolved gases were extracted into glass ampoules and were subsequently introduced into a vacuum system to remove gases other than helium. After this separation, helium isotopes (^{3}He and ^{4}He) were analyzed with the dual-collector noble gas mass spectrometer. The excess ^{3}He in seawater samples (relative to atmospheric composition) is expressed in terms of $\delta^3\text{He}\ (\%) = (R/R_{atm} - 1) \times 100$, where R and R_{atm} represent the isotopic ratios of ^{3}He/^{4}He in the seawater and atmosphere, respectively (Lupton, 1998). The standard error (1σ) lies within the limit of 0.43% for isotopic measurement. The excess helium (Δ^3He) is calculated for hydrothermal plume waters by subtracting the average regional background water helium-3 concentrations from the actual plume helium-3 concentrations ($\Delta^3\text{He} = [^3\text{He}]_{sample} - [^3\text{He}]_{background}$).

Samples for methane concentration and stable carbon isotopic composition were directly drawn from Niskin bottles using Tygon tubing inserted into 125 mL borosilicate glass bottles allowing the bottle to be flushed with >250 mL of sample. Upon overflowing the bottle with the sample, the tubing was slowly removed to ensure that no air bubbles were present in the bottles. Each sample was preserved with 1 mL of saturated mercuric chloride solution, and the bottle was capped with a butyl rubber stopper and aluminum crimp seal. All samples were stored at 4°C until shore-based analysis. The methane concentration and stable isotopic ratios were measured by using an isotope-ratio mass spectrometer (IRMS) coupled with a gas chromatograph (GC) at Nagoya University, Japan. The detailed analytical method for measuring methane concentration and stable carbon isotopes was described in Hirota et al. (2010) and Tsunogai et al. (2020). Analytical precisions were around ±3% for methane concentrations and 0.2‰ for $\delta^{13}\text{C-CH}_4$.

After completing the sampling for helium and methane, the remaining seawater was directly filtered through 0.45-micron size cellulose ester filter papers (Millipore) using diaphragm pumps. One liter of filtered seawater was acidified to pH less than 2.0 using ultra-pure nitric acid (Merck) for further shore-based laboratory analysis of manganese and iron. The DMn concentrations were measured by in-line pre-concentration on resin-immobilized 8-hydroxyquinoline and spectrophotometric detection described by Resing and Mottl (1992). The DFe concentrations were measured by a seaFast online pre-concentration system integrated with a high-resolution inductively coupled plasma mass spectrometer (HR-ICPMS) at the University of Washington. The accuracy and precision were better than 5% and 2% for both manganese and iron.

At P5 station, plume particles from ~200 m above the seafloor (2570 m) were collected onto 0.45-micron cellulose ester filter paper. The filter along with particles was subjected to visual observations under JEOL JSM-5410LV Scanning Electron Microscope (SEM) at National Centre for Polar and Ocean Research, India. A small portion of the filter paper was carefully sliced and fixed on aluminum stubs and then coated with a thin layer of platinum for studying morphological features. Elemental compositions of individual grains were determined by Energy Dispersive X-ray Spectrometrometry. The operating conditions were generally maintained within the limit of 18 keV, with a magnification range from 1600x to 20000x. The Wavelength Dispersive Spectra (WDS) of the same sample was generated using CAMECA SX-FIVE electron microprobe (EPMA) at National Centre for Polar and Ocean Research, India. The analysis was performed with an accelerating voltage of 15 keV. Focused electron beams were used with a variable probe current ranging from 5 to 15 nA. Full spectrometer scanning was done using TAP, PET, LPET, and LLIF crystals in all analyses. The required spectra and corresponding peak positions for individual elements were identified from the spectral database using SX peak-sight 6.4 software.

3. Results

3.1. Physical Tracer: Turbidity Signals

The two vertical stations, CTD-17-P5 and CTD-17-P8 (hereafter termed as P5 and P8, respectively) and the tow-yo (T-5) CTD operations showed very high turbidity signals between 2300 and 2650 m (Srinivas Rao & Kurian, 2018), with two distinct layers concentrated at 2400 m and 2570 m (Figures 3 and 4). In the P5 station, a turbidity anomaly of 0.07 ΔNTU was observed between 2320 and 2500 m and 0.13 ΔNTU between 2510 and

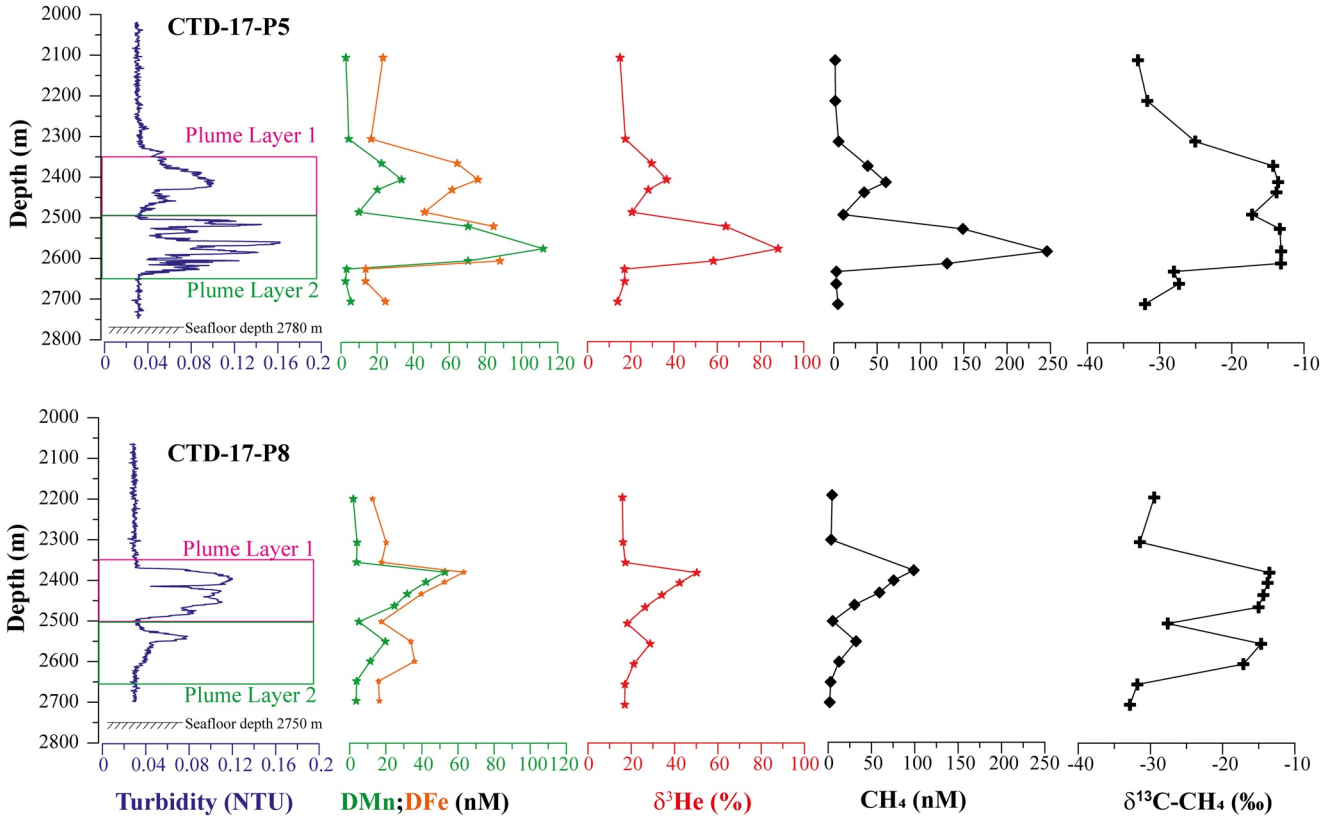

Figure 3. Vertical profiles of turbidity, dissolved manganese (DMn) and iron (DFe), δ^3He, methane (CH_4) and its stable isotopic composition (δ^{13}C-CH_4) in two plume layers 1 & 2 of two CTD stations, P5 and P8.

2650 m. Whereas, in P8, a turbidity anomaly of 0.09 ΔNTU was observed between 2400 and 2550 m and 0.05 ΔNTU between 2550 and 2700m. The maximum turbidity anomalies were observed in plume layers 1 and 2 for P8 and P5, respectively. Based on variable turbidity signals in different depth layers, we discriminate two plume layers as plume layer 1 (between 2320 and 2500m) and plume layer 2 (between 2500 and 2700 m). Each plume layer has a thickness of around 150 m (Figure 3).

3.2. Chemical Tracers: Helium (δ^3He), Methane (CH_4), Dissolved Manganese, and Iron Concentrations (DMn and DFe)

Seawater samples collected from plume layers 1 and 2 of both P5 and P8 stations show high concentrations of methane, dissolved trace metals (DMn and DFe), and significant changes in the isotopic ratios of helium (δ^3He) and methane (δ^{13}C-CH_4) (Figure 3; Table 1). The variations in concentrations will be discussed in relation to the plume layers in the following subsections.

3.2.1. Plume Layer 1 From 2350 to 2500 m

In plume layer 1, δ^3He values, CH_4, DMn and DFe concentrations vary (plume maxima) from 36% to 50%, 59–98 nM, 33–53 nM and 63–76 nM respectively (Table 1). Among the two stations, the maximum concentrations were observed at 2375 m of P8 with 98 nM of CH_4, 52.82 nM of DMn, and 63.16 nM of DFe and a value of 50.25% for δ^3He; (Figure 3). These concentrations are quite high when compared to the regional ambient seawater concentrations of CH_4 (~0.6 nM; Kawagucci et al., 2008), DMn and DFe (≤1 nM; Gallant & Von Damm, 2006) and value of δ^3He (~15%; Takahata et al., 2018). However, in the present study, the concentrations of seawater samples collected above the plume layer 1 (2100 and 2200 m) are relatively high compared to regional values. They vary from 15% to 16% of δ^3He, 1.6–4.5 nM of CH_4, DMn of 1.9–2.7 nM, and DFe of 12–24 nM, respectively (Figure 3 and Table 1). The background concentrations were found to be high for P8 (15.95% of ^{3}He; 4.5 nM of CH_4; and 1.95 nM of DMn; Table 1) when compared to P5. Geochemical ratios such

Table 1
Concentrations of Dissolved Manganese, Iron, Helium (δ^3He), Methane and Stable Carbon Isotope Ratios and Geochemical Ratios of Hydrothermal Plumes for the CTD Stations CTD-17-P5, CTD-17-P8, and Tow-Yo-T5

Depth (m)	DMn (nM)	DFe (nM)	^{3}He (fM)	δ^3He (%)	Δ^3He	CH_4 (nM)	δ^{13}C-CH_4 ‰	CH_4/Mn	CH_4/Δ^3He (mol/mol × 10^6)	Mn/Δ^3He	Fe/Δ^3He
CTD-17-P5 Latitude: 24°48′37″S, Longitude: 69°52′48″E, Depth: 2780 m											
1400	NA	NA	NA	NA	NA	0.8	−43.0	–	–	–	–
2100	2.68	23.24	2.98	15.02	0	1.6	−33.0	0.58	–	–	–
2200	NA	NA	NA	NA	NA	1.7	−31.7	–	–	–	–
2300	4.24	16.64	3.09	17.51	0.09	5.4	−25.1	1.27	60	47	185
2360	22.42	64.31	3.47	29.63	0.47	39	−14.3	1.74	83	48	137
2400	**33.55**	**75.89**	**3.69**	**36.59**	**0.69**	**59**	**−13.6**	**1.79**	**87**	**49**	**110**
2425	20.15	61.61	3.42	28.09	0.42	35	−13.8	1.73	83	48	147
2480	9.82	46.26	3.18	20.59	0.18	11	−17.2	1.11	61	55	257
2515	70.37	84.48	4.62	63.91	1.62	149	−13.4	2.12	92	43	52
2570	**112**	NA	**5.54**	**88.09**	**2.54**	**246**	**−13.2**	**2.20**	**97**	**44**	-
2600	70.37	88.00	4.40	58.21	1.35	131	−13.2	1.86	93	50	63
2620	3.11	13.67	3.07	17.14	0.07	2.9	−28.0	0.94	42	44	195
2650	2.49	13.58	3.07	17.21	0.07	2.8	−27.3	1.11	40	36	194
2700	5.39	24.57	3.58	13.94	0.58	4.7	−32.0	0.86	80	93	424
CTD-17-P8 Latitude: 24°48′41″S, Longitude: 69°52′53″E, Depth: 2750 m											
2190	1.95	12.65	3.04	15.95	0.04	4.5	−29.5	2.33	114	49	316
2300	4.09	20.23	3.03	16.23	0.03	3.4	−31.5	0.84	114	136	674
2350	3.82	17.64	3.06	17.30	0.06	NA	NA	-	-	64	294
2375	**52.82**	**63.16**	**4.16**	**50.25**	**1.16**	**98**	**−13.5**	**1.87**	**85**	**46**	**54**
2400	42.25	52.55	3.89	42.38	0.89	75	−13.8	1.79	85	47	59
2430	31.85	36.69	3.67	34.13	0.67	59	−14.4	1.86	88	48	59
2460	24.81	55.70	3.36	26.40	0.36	30	−15.0	1.22	84	69	155
2500	5.10	17.54	3.11	18.17	0.11	5.2	−27.6	1.02	47	46	159
2550	**19.75**	**33.86**	**3.34**	**28.76**	**0.34**	**32**	**−14.7**	**1.63**	**94**	**58**	**100**
2600	11.37	35.93	3.22	21.18	0.22	12	−17.1	1.10	57	52	163
2650	3.81	16.02	3.11	17.10	0.11	2.8	−31.8	0.74	26	35	146
2700	3.58	16.42	3.15	17.04	0.15	1.8	−32.8	0.50	12	24	109
Tow-Yo-T5 from 24°49′35″S, 69°54′08″E to 24°48′20″S, 69°52′23″E											
2567	16.24	48.20	3.28	23.82	0.28	23	−15.3	1.39	80	58	172
2527	27.24	69.58	NA	NA	NA	40	−14.5	1.49	-	-	-
2428	30.00	73.34	3.47	29.71	0.47	39	−14.9	1.30	83	64	156
2490	52.00	115	3.97	47.61	0.97	93	−13.7	1.80	96	54	119

Note. NA: Not Analyzed; Δ^3He is calculated by considering the excess helium-3 in plumes by subtracting the background ^{3}He concentration of 3.00 fM. Bold value represents the maximum values observed in each plume layers 1 and 2.

as CH_4/Mn, CH_4/Δ^3He, Mn/Δ^3He and Fe/Δ^3He at the P8 plume maxima (plume layer 1) are 1.87, 85 × 10^6, 46 × 10^6, and 54 × 10^6 respectively (Table 2).

3.2.2. Plume Layer 2 From 2500 to 2650 m

In plume layer 2, the concentrations (plume maxima) of CH_4, DMn, DFe and δ^3He value vary from 32 to 246 nM, 19–112 nM, 33–85 nM, and 28%–88%, respectively (Table 1), with maximum concentrations at 2570 m of P5

Table 2
Comparison of δ^{13}C-CH_4 (‰) and CH_4/Mn, $CH_4/^3$He, Mn/^{3}He and Fe/^{3}He of sCIR 24°49'S Plumes With Global Vent Fluids

Ridge	Vent field	Description	δ^{13}C-CH_4 (‰)	CH_4/Mn	$CH_4/^3$He ×10^6	Mn/^{3}He ×10^6	Fe/^{3}He ×10^6	References
Hydrothermal systems with seawater circulation through ultramafics								
sCIR	sCIR-24°49'S	Plumes	−13.1 to −13.5	1.8–2.2	85–97[a]	44–46[a]	[b]52–54[a]	This study
MAR	Rainbow	Vent	−15.8	1	100	90	960	Jean-Baptiste et al. (2004), Douville et al. (2002), Charlou et al. (1998), Charlou et al. (2002)
	Logatchev	Vent	−13.6	10	167	16	115	Jean-Baptiste et al. (2004), Douville et al. (2002), Charlou et al. (2002), Schmidt et al. (2007), Keir et al. (2009)
Hydrothermal systems with seawater circulation through basalts								
MAR	Lucky Strike	Vent	−12.7 to −13.7	2	65	25	31	Charlou et al. (2000) , Jean-Baptiste et al. (1998), Von Damm et al. (1998)
	MenezGwen	Vent	−18.8 to −19.6	26	85	3.3	0.13	Charlou et al. (2000), Jean-Baptiste et al. (1998)
	TAG	Vent	−8.0 to −9.5	0.21	8.8	60	310	Charlou et al. (2000), Rudnicki and Elderfield (1992), Charlou et al. (1996), Campbell et al. (1988)
	Snake Pit	Vent	–	0.15	5	32	192	Douville et al. (2002), Charlou et al. (2002), Rudnicki and Elderfield (1992), Jean-Baptiste et al. (1991)
CIR	Kairei	Vent	−8.7 to −18	0.1 to 0.25	–	–	–	Gamo et al. (2001), Kumagai et al. (2008), Gallant and Von Damm (2006)
	Edmond	Vent	−13.5 to −17	0.17 to 0.29	–	–	–	Gallant and Von Damm (2006),Kumagai et al. (2008), Kawagucci et al. (2016)
	Solitaire	Vent	−18.0	0.55	–	–	–	Kumagai et al. (2008), Kawagucci et al. (2016)
	Dodo	Vent	−40.2	0.03	–	–	–	Kumagai et al. (2008), Kawagucci et al. (2016)
EPR	21°N	Vent	−15.0 to −17.6	0.07	5	77	134	Welhan and Craig (1983), Von Damm et al. (1985)
	13°N	Vent	−16.6 to −19.6	0.03	3	80	190	Merlivat et al. (1987), Bowers et al. (1988)
	11°N	Vent	–	0.02	1	51	147	Bowers et al. (1988), Kim (1984)
Hydrothermal systems with seawater circulation through sediment covered (or) influenced								
NW Pacific	Okinawa Trough	Vent	−30.8	23	1430	61	40	Ishibashi et al. (2014)
Arctic	Loki's Castle	Vent	−29.1	236	1589	6.7	1	Baumberger et al. (2016)

[a]Ratios of CH_4/Δ^3He; Mn/Δ^3He and Fe/Δ^3He are calculated by considering the excess helium-3 (Δ^3He) in plumes by subtracting the background ^{3}He concentration of 3.00 fM. [b]Fe/Δ^3He value at 2515 m of CTD-17-P5 station is considered.

(Figure 3). Very high δ^3He of 88% is observed at 2570 m of P5 and is the largest anomaly observed in the Indian Ocean (Gamo et al., 2015; Kawagucci et al., 2008; Ray et al., 2008, 2012, 2020; Takahata et al., 2018). In addition, background concentrations (below plume layer 2 and above the seafloor; 50–80 m) were found to be high for P5 (13.94% of δ^3He; 4.7 nM of CH_4; 5.4 nM of DMn and 24.57 nM of DFe when compared to P8. Geochemical ratios such as CH_4/Mn, CH_4/Δ^3He, Mn/Δ^3He and Fe/Δ^3He at the P5 plume maxima (plume layer 2) are 2.2, 97×10^6, 44×10^6, and 52×10^6 (Table 2). DFe concentration at plume maxima could not be measured because

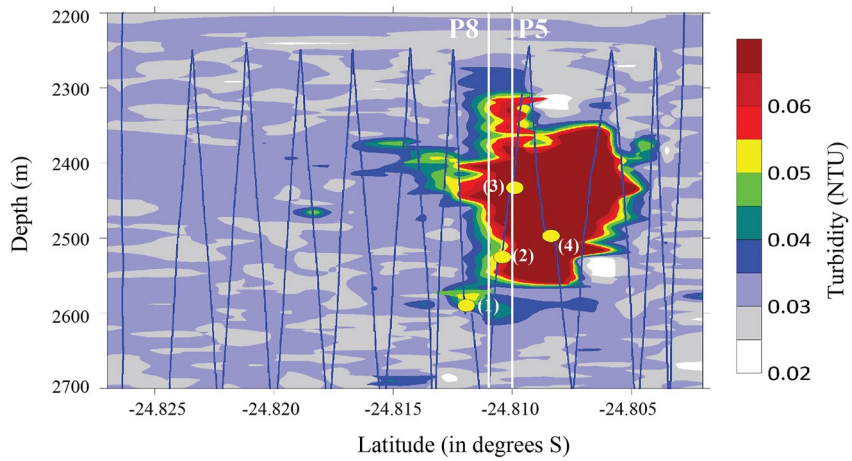

Figure 4. The turbidity profile during tow-yo CTD station (T5 in Figure 1C).

of sample contamination. So the next highest concentration (84.48 nM) measured at 2515 m depth was considered for the Fe/Δ^3He ratio (52×10^6).

3.3. Tow-Yo CTD Operation (T5) Between P5 and P8

A tow-yo CTD profile (T5 in Figure 1c) in the southeast-northwest direction between the P5 and P8 was undertaken to understand the extent of distribution of chemical species of hydrothermal plumes in the vicinity of active venting. The δ^3He, CH_4 and its stable carbon isotope composition, DMn concentrations are within the range of concentrations (except for DFe) measured at P5 and P8 (Figure 4). However, the sample collected at 2490 m has elevated concentrations for each chemical tracer; interestingly, this is the boundary between plume layers 1 and 2 in P5 and P8.

3.4. Stable Carbon Isotope Ratios of Methane (δ^{13}C-CH_4) in Plume Layers 1 and 2

The carbon isotope ratios of methane (δ^{13}C-CH_4) in plume layers 1 and 2 (plume maxima) vary from −13.2‰ to −14.7‰ (Figure 3 and Table 1). In plume layer 1, at 2375 m, CH_4 = 98 nM, the isotopic composition was −13.5‰. However, in plume layer 2, 2570 m, CH_4 = 246 nM with the isotopic composition −13.2‰. It is very interesting to note that the sample collected from 2480 m at P5 has a relatively low CH_4 concentration (10 nM) with an isotopic composition (−17.2‰) that is quite close to the samples with much higher CH_4 concentrations. Samples collected during the tow-yo CTD operation (T-5) are slightly different and vary from −13.7‰ to −15.3‰ (Table 1). The background samples collected above and below the plume layers 1 and 2 show a similar isotopic composition of −29.5 to −33.0‰ even though the methane concentrations were high, 1.6–4.7 nM (Figure 3 and Table 1).

3.5. Morphological and Mineralogical Features of Plume Particulates

Micro textures of plume particulates were studied using scanning electron microscopy, and the generated back scatter images are given in Figure 5. The plume particles have distinct morphological features, including fine grains of barite and pyrite and relatively bigger chalcopyrite, Fe-Mg-silicates, along with Fe-oxyhydroxides. X-ray energy dispersive spectroscopic and wavelength-dispersive spectroscopic results of plume particles and their relative compositions confirm that they are hydrothermal sulfides and sulfate. In addition, siliceous microfossils, silicoflagellates have been observed on the filter.

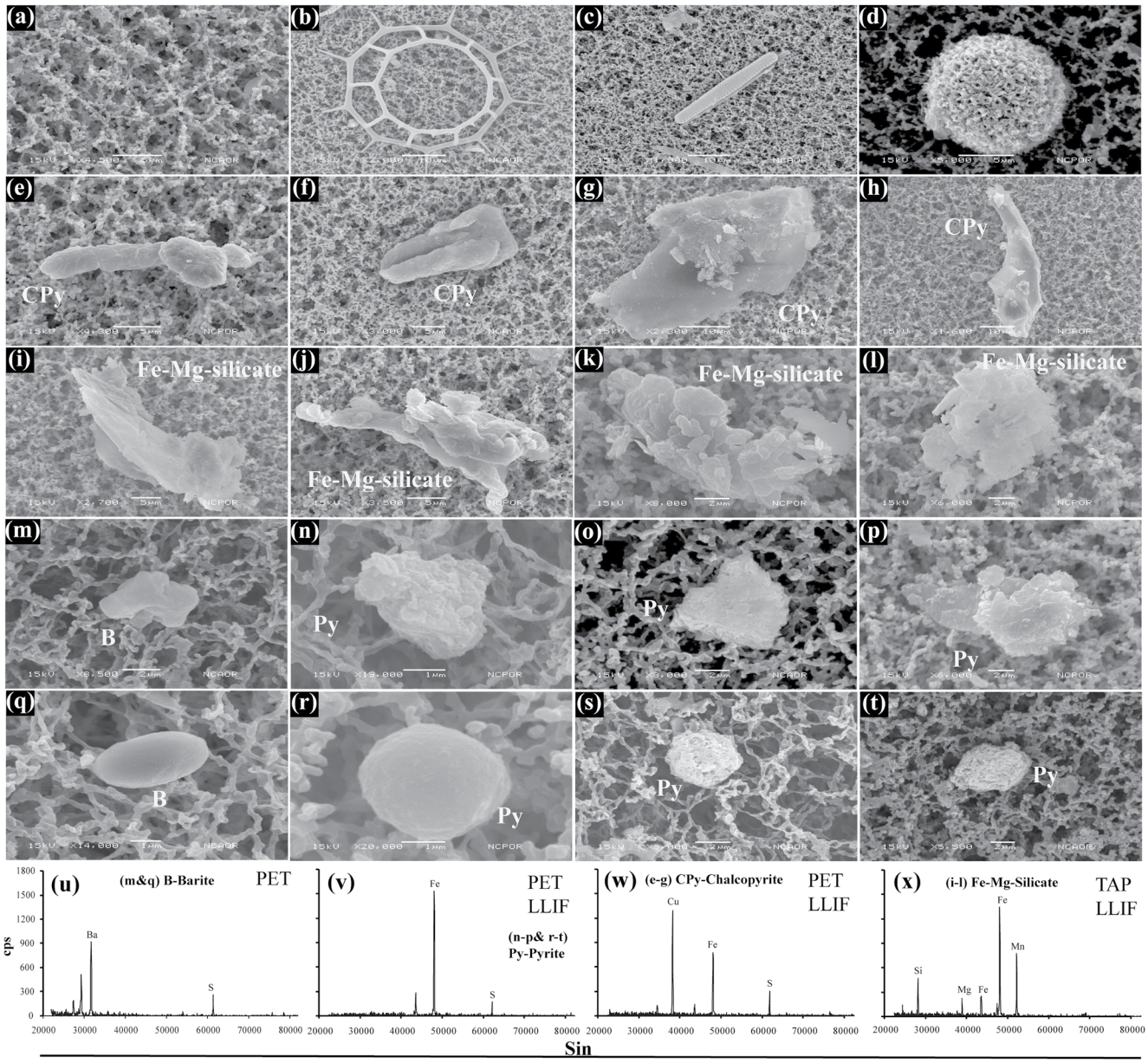

Figure 5. Scanning Electron Microscope images of blank filter material (a), micro fossils (b, c and d) and plume particulates (e–t) collected from the 2570 m at CTD station P5. Large particles (e–h) are mainly composed of chalcopyrite and small particles (m–t) are pyrite, and barite. However the platy particles (i–l) are Fe-Mg-silicates. The representative spectra of barite (u), pyrite (v) and chalcopyrite (w) and Fe-Mg-Silicate (x) are shown at the bottom.

4. Discussion

4.1. Physical and Chemical Anomalies in the Water Column: Evidences for the High-Temperature Fluid Venting

Turbidity signals observed in the deep waters along the mid-ocean ridges are primarily associated with seafloor hydrothermal activity. When high temperature (>300°C) fluids emitted from hydrothermal vents come in contact with oxygen-rich cold seawater, a particle-rich cloud is formed in the water column and is known as hydrothermal plume (German & Seyfried, 2013). In the present study, high turbidity anomalies (ΔNTU) in deep waters (compared to background value) indicate hydrothermal sources (Figure 3; Srinivas Rao & Kurian, 2018). The turbidity values of both plume layers 1 and 2 are comparable with other known hydrothermal plumes along the global mid-oceanic ridges. The thickness of both plume layers is about 150 m with the first plume between 2350

and 2500 m and the second plume between 2500 and 2650 m. The maximum turbidity anomaly (ΔNTU = 0.13) is observed at 2570 m in plume layer 2 of P5, followed by 2375 m in plume layer 1 of P8 (ΔNTU = 0.09). These high turbidity values are clear indications of excess suspended particles precipitated from the reaction of reduced hydrothermal fluids with oxygen-rich seawater (Baker et al., 2010).

Both the plume layers 1 and 2 have high concentrations of trace metals (DMn and DFe), methane (CH_4), and high values of δ^3He when compared to their background seawater concentrations (Figure 3). In plume layer 1, maximum concentrations were observed at 2375 m in P8 and plume layer 2 at 2570 m in P5. Anomalously high concentrations of metals, gases, and turbidity in the water column establish the presence of plumes generated through hydrothermal activities. A sharp increase in dissolved trace metals and gas concentrations of plumes layers 1 and 2 at P8, and P5 indicate the possibility of nearby venting. These values are comparable to concentrations reported for hydrothermal plumes found in the Indian Ocean and elsewhere in global oceans (Boulart et al., 2017; Fang & Wang, 2021; Gamo et al., 2015; Gharib et al., 2005; González-Santana et al., 2020; Haalboom et al., 2019; Kawagucci et al., 2008; Ray et al., 2012, 2020; Resing et al., 2009; Schmid et al., 2019; Wang et al., 2012; You et al., 2014; Zhu et al., 2008 and references therein). The δ^3He (88%) at 2570 m at P5 is the highest reported hydrothermal plume value in the Indian Ocean (Table 1) when compared to hydrothermal plumes above Solitaire vent field (δ^3He = ∼56%; Kawagucci et al., 2008). This may reflect that this sample was collected close to the source.

Samples (depths indicated in italics in Table 1) collected above and below the plumes at P5 and P8 show relatively high concentrations of trace metals and gases when compared to regional background values (Gallant & Von Damm, 2006 and references there in). The observed high concentrations above the plume layer 1 might be because of variable plume height with time or they might be associated with the shallow topography of the axial walls which reach 2100–2200 m in to both the east and west of the axial valley. The concentrations below plume layer 2 are also relatively high (compared to regional background values) indicating possible contribution from diffuse flows associated with high-temperature active venting.

The stable carbon isotope ratios of methane (δ^{13}C-CH_4) in the plume layers shows heavier isotope enrichment (Figure 3 and Table 1) consistent with vent fluids ($\delta^{13}C = -9$ to $-20‰$) found elsewhere along the global mid-oceanic ridge (Charlou et al., 1998, 2000; Douville et al., 2002; Gamo et al., 2001; Kawagucci et al., 2016; Keir et al., 2009; Kumagai et al., 2008; Schmidt et al., 2007; Von Damm et al., 1998) but distinctly different from sediment-influenced ($\delta^{13}C = -55$ to $-20‰$) hydrothermal systems (Baumberger et al., 2016; Gamo et al., 2010; Ishibashi et al., 2014; Kawagucci et al., 2010). Although there is a huge variation in maximum methane concentrations (32–246 nM) of both plume layers 1 and 2, the carbon isotope composition does not show much variation (only 1.5‰, Table 1). This is likely because the methane concentration in the plume is much greater than the surrounding seawater. Thus, changes in isotopic composition due to entrainment of and mixing with ambient seawater are not observed at these methane concentrations. In addition, microbial methane oxidation (Tsunogai et al., 2000) produces enrichment of the heavier isotope in the residual plume water with increasing distances from its source region. To test this hypothesis in the present study, we have calculated the changes, caused by microbial methanotrophic activity, in both methane concentrations and its carbon isotope compositions by considering the highest concentration of methane (246 nM) and its carbon isotope composition ($\delta^{13}C = -13.2$; Table 1) in the plume. The calculated lines of kinetic isotopic effect of 1.004, 1.001 and 1.000 (Coleman et al., 1981; Gharib et al., 2005; Kawagucci et al., 2008; Sansone et al., 1999; Tsunogai et al., 2000) are given in Figure 6a. The measured carbon isotope composition of the plume samples does not fall on any of these KIE lines (Figure 6a). So the heavier isotope enrichment in plume layers 1 and 2 associated with high methane concentrations might be because of the proximity of active venting where its isotopic composition remains unchanged even after dilution of hydrothermal fluids rather than microbial methane consumption.

The isotopic ratios of CH_4 in samples above and below the plumes range from $-29‰$ to $-33‰$ (Table 1), similar to regional observations of deep seawater CH_4 isotopic ratios of $-32.5‰$ to $-35‰$ (Kawagucci et al., 2008; You et al., 2014). The sample collected at 1400 m in the present study area has a CH_4 concentration of 0.77 nM with an isotopic ratio of $-43.0‰$. Therefore, this data point can be used as another non-hydrothermal end-member in Figure 6a. The background samples collected above and below plume layers are isotopically light but do not fall on the simple mixing line (Figure 6a). The Keeling plot analysis (Keeling, 1958; Tsunogai et al., 1998) of plume samples does not fall on a simple mixing between the plume and seawater. Hence, two theoretical mixing lines (You et al., 2014) were generated (Figure 6b) by adding incremental amounts of methane with $\delta^{13}C = -13.2‰$

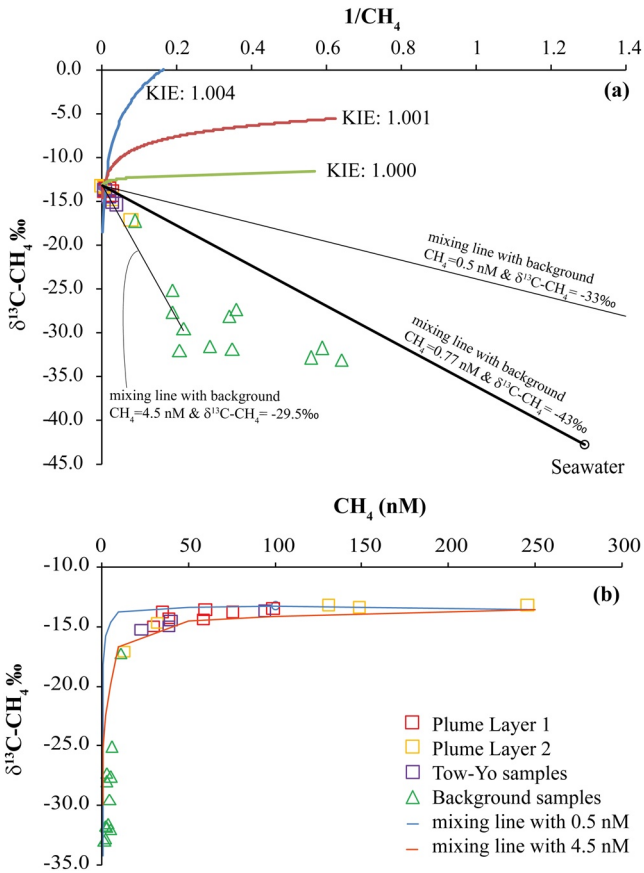

Figure 6. (a) Keeling plot of 1/[CH_4] versus stable carbon isotope ratios of methane ($\delta^{13}C$-CH_4) of water samples collected from CTD stations P5 & P8. A simple fluid and seawater mixing line was derived with the highest methane concentration of the plume with 246 nM and $\delta^{13}C = -13.3‰$ and ambient seawater methane concentration of 0.77 nM with $\delta^{13}C = -43‰$ (measured for sample collected at 1400 m of P5 station); seawater methane concentration of 0.5 nM with $\delta^{13}C = -33‰$ (Kawagucci et al., 2008) and also with enhanced seawater methane concentration of 4.5 nM with $\delta^{13}C = -29.5‰$ of sample collected from 2190 m of P8 station. (b) [CH_4] versus stable carbon isotope ratios of methane ($\delta^{13}C$-CH_4) for samples of P5 & P8. A blue line was generated by adding incremental amounts of methane with $\delta^{13}C = -13.3‰$ to ambient seawater methane concentration of 0.5 nM with $\delta^{13}C = -33‰$ (You et al., 2014). The red line was generated by adding the same methane with $\delta^{13}C = -13.3‰$ to background seawater methane concentration to 4.5 nM with $\delta^{13}C = -29.5‰$.

to regional seawater methane concentration of (a) 0.5 nM with $\delta^{13}C = -33‰$ and (b) 4.5 nM with $\delta^{13}C = -29.5‰$ (measured at 2190m at P8). The isotope ratio of all samples falls on the mixing line derived with ambient seawater methane concentration of 4.5 nM (Figure 6b), indicating that though the particles settle down, the dissolved components of hydrothermal plumes remain in the water column.

It is very interesting to observe high concentrations of manganese (5.10–9.82 nM), iron (17.54–46.26 nM), methane (5.2–11 nM) and helium values (18%–21%) for samples collected from 2480 m at P5 and 2500 m at P8 (Table 1) in the absence of turbidity anomaly (Figure 3). However, distinct isotope ratios −17.2‰ for P5 and −27.6‰ for P8 stations (Table 1) are observed. The isotope ratio of −17.2‰ for P5 is much similar to the highest methane concentration (246 nM) with isotope ratio of −13.2‰ observed for plume layer 2 maxima (Table 1). Although manganese, iron and methane concentrations are high for both P5 and P8, the distinct isotope ratios observed for sample collected from 2480 m at P5 may indicate that the plume in P5 is less diluted when compared to P8 and may infer the proximity to the active venting source.

The mixing of hydrothermal fluids with ambient seawater generates particle clouds that contain metallic sulfides, sulfates, oxides, and oxyhydroxides (Feely et al., 1990; Feely, Gendron, et al., 1994; Feely, Massoth, et al., 1994). Most of the sulfides (pyrite, chalcopyrite, sphalerite and others) form chimneys when the hot hydrothermal fluids come in contact with the cold ambient seawater. In the buoyant stage of the plume, iron sulfides, pyrite, are commonly observed (Feely et al., 1990; Findlay et al., 2019; Gartman et al., 2014; Mottl & McConachy, 1990; Yücel et al., 2011), while oxides are found in non-buoyant plumes (Edmonds & German, 2004; Feely et al., 1998; Ray et al., 2012, 2017 and references therein). Relatively large particles (>30 μm) of sphalerite, wurtzite, pyrite, pyrrhotite, barite, chalcopyrite and cubanite have been observed in the first few meters (10–20 m) of the hydrothermal plume at Juan de Fuca Ridge (Feely et al., 1987). However, filaments of biogenic origin of Mn-Fe-Si phase, orb-like particles of Fe-Mn-Si phase, barite, anhydrite, amorphous iron oxide, and unidentified Si-Fe rich phase along with biogenic detritus have been observed in the non-buoyant hydrothermal plumes in the eastern Manus Basin (Ortega-Osorio & Scott, 2001). In addition, platy-shaped Mg-rich silicates (talc) are observed in non-buoyant hydrothermal plumes in the Carlsberg Ridge (Ray et al., 2012, 2017) and inferred that they might have been originated from the hydrothermal system hosted by ultramafic rocks.

In the present study, the particles have different morphological features (Figure 5), and their chemical composition shows that they are mainly sulfides (pyrite, and chalcopyrite), sulfates (barite), and Fe-oxyhydroxides. Three types of particle morphologies were observed in the plume (a) irregular shaped bigger size particles (~20–50 μm), mainly chalcopyrite (Figures 5e–5h), (b) platy shaped Mg-rich silicates (Figure 5i-5l), and (c) fine shaped and smaller size sulfides (~3–9 μm) of pyrite and sulfates of barite (Figure 5m–5t). A high abundance of sulfide particles in the water column clearly indicates that these particles are associated with high-temperature hydrothermal venting or erosion of sulfides from the chimney walls by ascending fluids. Polymetallic sulfide nano particulates and iron-containing silicate particles have been widely reported in the Rainbow, TAG, Snakepit, and EPR 9°N hydrothermal systems (Findlay et al., 2019; Gartman et al., 2014; Yücel et al., 2011). In addition to sulfides, hydrothermal sulfates such as barite is also observed in the present plume particles is much similar to Rainbow vent field where low-soluble hydrothermal sulfates are observed in the residual fraction of sediment core (Chavagnac et al., 2005). Although Fe-oxyhydroxides are commonly observed in near- and far-field hydrothermal plumes, the

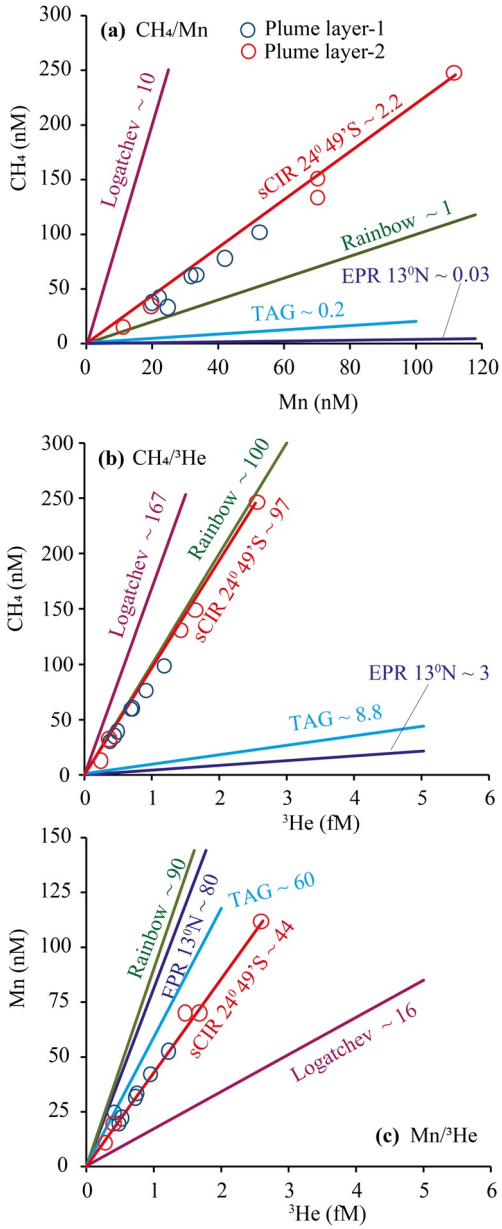

Figure 7. Interrelation plots of conservative helium (^{3}He) and quasi-conservative (CH_4 and Mn) elements (a) CH_4 versus Mn; (b) CH_4 versus ^{3}He and (c) Mn versus ^{3}He against plot of known vent fields of Pacific and Atlantic Ocean's Mid-Oceanic Ridges.

presence of sulfides, sulfates and platy-shaped Fe-Mg-silicates (talc) likely come from high-temperature hydrothermal fluid venting in the vicinity.

4.2. Conservative to Quasi-Conservative/Non-Conservative Nature of Elements: Implication on Water-Rock Interactions

Hydrothermal fluids are enriched in helium, methane and manganese because of subsurface water-rock reactions in high-temperature reaction zone. However, among these three, helium is termed as conservative in nature because of its non-reactivity to any biological process; whereas, the other two, methane and/or manganese, are reactive to biological processes and termed as quasi-conservative (Lam et al., 2004; Lupton, 1995; Tsunogai et al., 2000 and references therein). The elemental ratios of conservative helium and quasi-conservative methane and/or manganese can be used to identify the sources of methane. Excess helium (Δ^3He) is calculated for this purpose by removing the regional background seawater helium-3 concentrations (3.0 fM) from actual helium-3 concentrations in the plume waters.

CH_4/Mn, $CH_4/^3$He, Mn/^{3}He (Figures 7a–7c), and Fe/^{3}He ratios in hydrothermal systems discovered in the Arctic, Pacific, and Atlantic Oceans are summarized in Table 2. These $CH_4/^3$He ratios range between 1 and 1590×10^6 (Baumberger et al., 2016; Ishibashi et al., 2014; Kawagucci et al., 2008 and references therein) and includes basalt and ultramafic hosted systems along with sediment influenced ones. The lowest $CH_4/^3$He ratios ($<10 \times 10^6$) are observed at systems with basaltic substrates, and the highest ratios of $CH_4/^3$He ($>1400 \times 10^6$) are found in sediment-covered/influenced systems. However, ratios between these values ($60–170 \times 10^6$) are found in systems where serpentinization of ultramafic rocks occurs (Charlou et al., 2002). Elevated methane generally originates from one or more of the following processes, (a) thermal decomposition of organic matter (Lilley et al., 1993; Sakai et al., 1990), (b) microbial methanogenesis (Whiticar, 1999), (c) serpentinization of ultramafic rocks (Charlou et al., 2002; Schmidt et al., 2007), (d) phase separation (Ishibashi et al., 1997) and (e) volatile input by magmatic perturbation (Ishibashi et al., 1997; Stüben et al., 1992). Both $CH_4/^3$He and CH_4/Mn ratios are high where methane is produced by the first three processes. In fluids of a magmatic origin or when phase separation segregates volatiles from metals, the CH_4/Mn ratio is high; meanwhile, as components of the gas phase, CH_4 and ^{3}He follow similar trends (Charlou et al., 2000; Gharib et al., 2005; Ishibashi et al., 1988, 1997; Kawagucci et al., 2008; Mottl et al., 1995; Schmidt et al., 2007; Stüben et al., 1992).

Hydrothermal systems involved in seawater circulation through ultramafic/gabbroic rocks produce methane enrichment in fluids, leading to high methane/helium ratios (Figure 8; Table 2). In the present study, the CH_4/Δ^3He ratio of both plume layers 1 and 2 varies from $85–87 \times 10^6$ and $94–97 \times 10^6$ (Table 1). These ratios are close to Logatchev and Rainbow hydrothermal systems in slow-spreading MAR (Charlou et al., 2000, 2002; Jean-Baptiste et al., 2004; Schmidt et al., 2007) and different from the hydrothermal systems in the fast-spreading East Pacific Rise (Gharib et al., 2005; Haymon et al., 1993; Merlivat et al., 1987; Welhan & Craig, 1983) (Table 2). The maximum observed CH_4/Δ^3He ratio for plume layers 1 and 2 is 85×10^6 and 97×10^6 (Table 2; Figure 7b). Therefore, high methane concentrations in these plumes likely originated from the seawater circulation through ultramafic rocks; the elevated CH_4/Mn ratios of more than 2 (Figure 7a) substantiates this argument.

The end-member methane concentrations for plume layers 1 and 2 are calculated by considering the CH_4/Δ^3He ratios and global average end-member ^{3}He concentration of 17.1 pmol/kg for matured sites (Jean-Baptiste et al., 2004). If we assume conservative mixing, the estimated methane concentrations are very high (0.4 mmol/kg

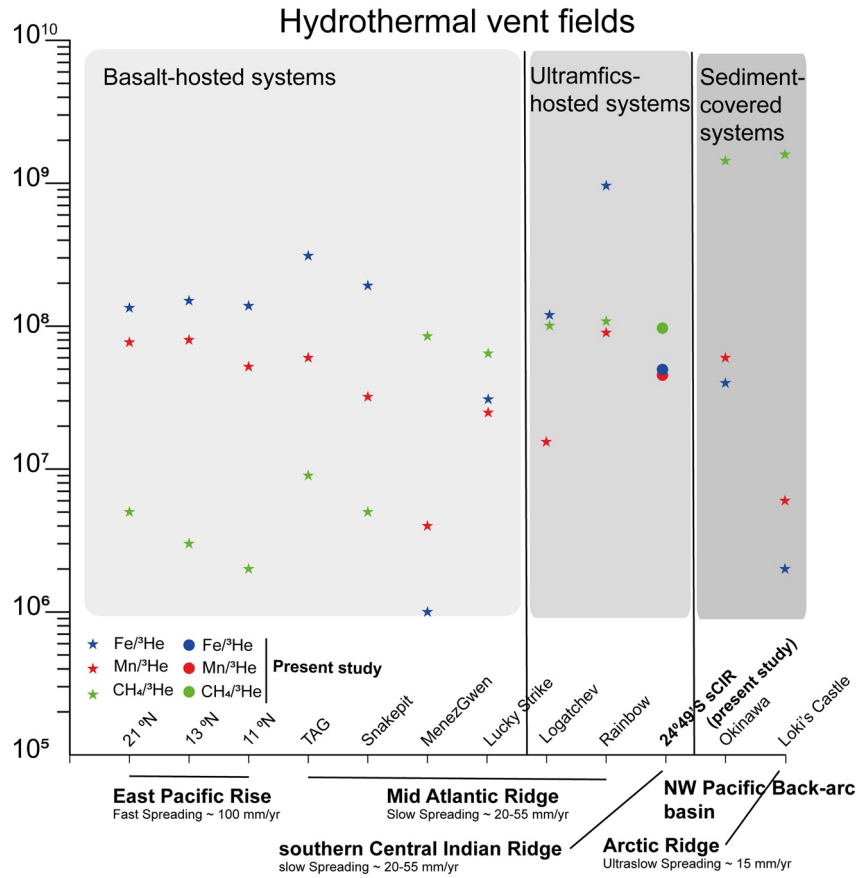

Figure 8. Fe/^{3}He; Mn/^{3}He and CH_4/^{3}He ratios of hydrothermal vent fluids collected from fast spreading (~100 mm/yr) East Pacific Rise, slow spreading (~25–55 mm/yr) Mid-Atlantic Ridge and ultraslow spreading (~15 mm/yr) Arctic ridge along with NW Pacific back-arc basin are compared with the present study. Data source is same as Table 2.

and 0.76 mmol/kg) and comparable with hydrothermal systems with fluid circulation through ultramafic lithologies, for example, Rainbow, Logatchev; (Charlou et al., 2002; Schmidt et al., 2007). This is similar to end-member fluids from the Longqi hydrothermal fields along the Southwest Indian Ridge (CH_4 = 0.38 mmol/kg; Ding et al., 2017; Ji et al., 2017; Yue et al., 2019) where methane enrichments were the result of reaction path of more than 6 km (Tao et al., 2020).

High-temperature hydrothermal fluids, either basalt or ultramafic hosted, don't show much variation in the metal to helium ratios (Figure 8; Table 2) and indicates that both Fe and Mn co-vary depending on the substrate rock type (in both recharge and reaction zones) and depends on the temperature and pressure of the reaction zone (Gallant & Von Damm, 2006; Kelley & Shank, 2010; Nakamura et al., 2009). High metal concentrations in Rainbow and Logatchev fluids were the result of high-temperature hydrothermal fluids reacting with ultramafic rocks (Charlou et al., 2000; Douville et al., 2002; Schmidt et al., 2007). Whereas low metal concentrations in MenezGwen fluids are mainly due to that system's low temperature and pressure (Charlou et al., 2000). In the present study, the Fe/Δ^3He and Mn/Δ^3He ratios of plume layers 1 and 2 (maxima) are almost in the same range, ~44–54 × 10^6 (Table 2) and are quite comparable with global high-temperature vent fluids of both basalt and ultramafic hosted systems. The enrichment of volatiles in the plumes, as shown by CH_4/Δ^3He and CH_4/Mn, indicate the ultramafics influence. These findings suggest a hydrothermal system with a high temperature and pressure reaction zone similar to Rainbow and Logatchev where the high-temperature hydrothermal fluids react with ultramafic rocks.

Although the concentrations of iron, manganese, methane, and helium values are different for both the plume layers 1 and 2 in P5 and P8, the geochemical ratios (CH_4/Mn; CH_4/Δ^3He; Fe/Δ^3He and Mn/Δ^3He) do not show

much variation at the plume maxima (Tables 1 and 2). These observations are consistent with single source-fluid chemistry with multiple venting.

5. Conclusions

Seawater samples for dissolved gases and trace metals were collected from two closely spaced (~300 m apart) vertical CTD stations, 24°48.62'S (CTD-17-P5) and 24°48.68'S (CTD-17-P8), in the southern Central Indian Ridge. High concentrations of manganese (19–112 nM), iron (33–76 nM), methane (32–246 nM), and δ^3He (28%–88%) values are observed in these two stations and provide evidence for the presence of hydrothermal plumes. Heavier carbon isotope ratios of methane (δ^{13}C-CH_4) in both plume layers, −13.2 to −14.7‰, are similar to the isotopic ratios of vent fluids elsewhere in the global ocean. The CH_4 maxima are not diluted enough by ambient seawater to change the isotopic ratio due to entrainment of ambient seawater. More importantly, the elevated methane values and the heavier carbon isotope ratios suggest that the methane has not had enough time to oxidize. This further suggest that the sampling locations must be close to an area of active venting, that has not as of yet, been unobserved. The presence of sulfides (pyrite and chalcopyrite), and sulfates (barite) in plume particles collected from the plume layer 2 of P5 (~200 m above the seafloor) also confirms the high-temperature fluid venting in the vicinity. The geochemical characteristics (CH_4/Mn ~ 1.8–2.2; CH_4/Δ^3He ~ 85–97 × 10^6; Mn/Δ^3He ~ 44–46 × 10^6 and Fe/Δ^3He ~ 52–54 × 10^6) of two hydrothermal plumes show that these plumes are enriched in dissolved gases and are generated from multiple vents with similar fluid chemistry possibly by seawater circulation through ultramafic rocks. Therefore the geochemical composition of hydrothermal plumes and recovery of ultramafic rocks provide evidence for a new ultramafic-hosted hydrothermal field near 24°49'S on the southern Central Indian Ridge.

Conflict of Interest

The authors declare no conflicts of interest relevant to this study.

Data Availability Statement

The entire geochemical data presented in this paper (Figures 3 and 6–8) is made available in Tables 1 and 2. Detailed data will be accessible through http://ramadda.npdc.ncpor.res.in/repository/entry/show?entryid=698b12be-8785-47ce-b17d-cc409725bf80.

Acknowledgments
We thank the Director of NCPOR, Ministry of Earth Sciences, for his support and encouragement. This work was carried out as a part of the ongoing "Hydrothermal Sulphides Studies program," with Grant No. MOES/EFC/28/2018-II, funded by the Ministry of Earth Sciences, Government of India. We acknowledge the masters, crew members, scientific and technical colleagues onboard ORV MGS Sagar for their support during the cruises. Thanks to Mr. Abhishek Tyagi for his onboard help and Dr. Shuhail for the preparation of maps. Thanks to Dr. Rahul Mohan and Miss. Sahina Ghazi, NCPOR, for their help in SEM-EDS analysis. SPL is grateful to InterRidge for the "InterRidge Student and Postdoctoral Fellowship 2017" award that enabled him to carry out trace metal analysis at the University of Washington (UW), USA. Thanks to Dr. R Bundy, UW, for providing laboratory space for setting up the Flow Injection system. We thank Dr. Camilla Wilkinson for the helium isotope analyses. We are thankful to the editor (Prof. Marie Edmonds); Dr. Kumagai H. and two anonymous reviewers for their constructive comments on the manuscript. This is NCPOR contribution no. J-32/2022-23, PMEL contribution 5362 and CICOES publication 2022-1214.

References

Baker, E. T., Martinez, F., Resing, J. A., Walker, S. L., Buck, N. J., & Edwards, M. H. (2010). Hydrothermal cooling along the eastern Lau Spreading Center: No evidence for discharge beyond the neovolcanic zone. *Geochemistry, Geophysics, Geosystems*, *11*(8). https://doi.org/10.1029/2010GC003106

Baumberger, T., Früh-Green, G. L., Thorseth, I. H., Lilley, M. D., Hamelin, C., Bernasconi, S. M., et al. (2016). Fluid composition of the sediment-influenced Loki's Castle vent field at the ultra-slow spreading Arctic Mid-Ocean Ridge. *Geochimica et Cosmochimica Acta*, *187*, 156–178. https://doi.org/10.1016/j.gca.2016.05.017

Boulart, C., Briais, A., Chavagnac, V., Révillon, S., Ceuleneer, G., Donval, J. P., et al. (2017). Contrasted hydrothermal activity along the South-East Indian Ridge (130°E–140°E): From crustal to ultramafic circulation. *Geochemistry, Geophysics, Geosystems*, *18*(7), 2446–2458. https://doi.org/10.1002/2016GC006683

Bowers, T. S., Campbell, A. C., Measures, C. I., Spivack, A. J., Khadem, M., & Edmond, J. M. (1988). Chemical controls on the composition of vent fluids at 13°–11°N and 21°N, East Pacific Rise. *Journal of Geophysical Research: Solid Earth*, *93*(B5), 4522–4536. https://doi.org/10.1029/jb093ib05p04522

Briais, A. (1995). Structural analysis of the segmentation of the Central Indian Ridge between 20°30′S and 25°30′S (Rodriguez Triple Junction). *Marine Geophysical Researches*, *17*(5), 431–467. https://doi.org/10.1007/BF01371787

Campbell, A. C., Palmer, M. R., Klinkhammer, G. P., Bowers, T. S., Edmond, J. M., Lawrence, J. R., et al. (1988). Chemistry of hot springs on the Mid-Atlantic Ridge. *Nature*, *335*(6190), 514–519. https://doi.org/10.1038/335514a0

Charlou, J. L., Donval, J. P., Douville, E., Jean-Baptiste, P., Radford-Knoery, J., Fouquet, Y., et al. (2000). Compared geochemical signatures and the evolution of Menez Gwen (35°50N) and Lucky Strike (37°17N) hydrothermal fluids, south of the Azores Triple Junction on the Mid-Atlantic Ridge. *Chemical Geology*, *171*(1–2), 49–75. https://doi.org/10.1016/S0009-2541(00)00244-8

Charlou, J. L., Donval, J. P., Fouquet, Y., Jean-Baptiste, P., & Holm, N. (2002). Geochemistry of high H_2 and CH_4 vent fluids issuing from ultramafic rocks at the Rainbow hydrothermal field (36°14′N, MAR). *Chemical Geology*, *191*(4), 345–359. https://doi.org/10.1016/S0009-2541(02)00134-1

Charlou, J. L., Donval, J. P., Jean-Baptiste, P., Dapoigny, A., & Rona, P. A. (1996). Gases and helium isotopes in high temperature solutions sampled before and after ODP Leg 158 drilling at TAG hydrothermal field (26°N, MAR). *Geophysical Research Letters*, *23*(23), 3491–3494. https://doi.org/10.1029/96GL02141

Charlou, J. L., Fouquet, Y., Bougault, H., Donval, J. P., Etoubleau, J., Jean-Baptiste, P., et al. (1998). Intense CH_4 plumes generated by serpentinization of ultramafic rocks at the intersection of the 15°20'N fracture zone and the Mid-Atlantic Ridge. *Geochimica et Cosmochimica Acta*, *62*(13), 2323–2333. https://doi.org/10.1016/S0016-7037(98)00138-0

Chavagnac, V., German, C. R., Milton, J. A., & Palmer, M. R. (2005). Sources of REE in sediment cores from the Rainbow vent site (36°14′N, MAR). *Chemical Geology*, *216*(3–4), 329–352. https://doi.org/10.1016/j.chemgeo.2004.11.015

Coleman, D. D., Risatti, J. B., & Schoell, M. (1981). Fractionation of carbon and hydrogen isotopes by methane-oxidizing bacteria. *Geochimica et Cosmochimica Acta*, *45*(7), 1033–1037. https://doi.org/10.1016/0016-7037(81)90129-0

DeMets, C., Gordon, R. G., & Argus, D. F. (2010). Geologically current plate motions. *Geophysical Journal International*, *181*(1), 1–80. https://doi.org/10.1111/j.1365-246X.2009.04491.x

Ding, J., Zhang, Y., Wang, H., Jian, H., Leng, H., & Xiao, X. (2017). Microbial community structure of deep-sea hydrothermal vents on the ultraslow spreading southwest Indian Ridge. *Frontiers in Microbiology*, *8*. https://doi.org/10.3389/fmicb.2017.01012

Douville, E., Charlou, J. L., Oelkers, E. H., Bienvenu, P., Jove Colon, C. F., Donval, J. P., et al. (2002). The rainbow vent fluids (36°14′N, MAR): The influence of ultramafic rocks and phase separation on trace metal content in Mid-Atlantic Ridge hydrothermal fluids. *Chemical Geology*, *184*(1–2), 37–48. https://doi.org/10.1016/S0009-2541(01)00351-5

Edmonds, H. N., & German, C. R. (2004). Particle geochemistry in the Rainbow hydrothermal plume, Mid-Atlantic Ridge. *Geochimica et Cosmochimica Acta*, *68*(4), 759–772. https://doi.org/10.1016/S0016-7037(03)00498-8

Fang, Z., & Wang, W. X. (2021). Size speciation of dissolved trace metals in hydrothermal plumes on the southwest Indian Ridge. *Science of the Total Environment*, 771. https://doi.org/10.1016/j.scitotenv.2021.145367

Feely, R. A., Baker, E. T., Lebon, G. T., Gendron, J. F., Massoth, G. J., & Mordy, C. W. (1998). Chemical variations of hydrothermal particles in the 1996 Gorda Ridge event and chronic plumes. *Deep-Sea Research Part II Topical Studies in Oceanography*, *45*(12), 2637–2664. https://doi.org/10.1016/S0967-0645(98)00087-3

Feely, R. A., Geiselman, T. L., Baker, E. T., Massoth, G. J., & Hammond, S. R. (1990). Distribution and composition of hydrothermal plume particles from the ASHES vent field at axial volcano, Juan de Fuca Ridge. *Journal of Geophysical Research*, *95*(B8), 12855–12873. https://doi.org/10.1029/jb095ib08p12855

Feely, R. A., Gendron, J. F., Baker, E. T., & Lebon, G. T. (1994). Hydrothermal plumes along the East Pacific Rise, 8 40′ to 11 50′N: Particle distribution and composition. *Earth and Planetary Science Letters*, *128*(1–2), 19–36. https://doi.org/10.1016/0012-821x(94)90023-x

Feely, R. A., Lewison, M., Massoth, G. J., Robert-Baldo, G., Lavelle, J. W., Byrne, R. H., et al. (1987). Composition and dissolution of black smoker particulates from active vents on the Juan de Fuca Ridge. *Journal of Geophysical Research*, *92*(B11), 11347–11363. https://doi.org/10.1029/jb092ib11p11347

Feely, R. A., Massoth, G. J., Trefry, J. H., Baker, E. T., Paulson, A. J., & Lebon, G. T. (1994). Composition and sedimentation of hydrothermal plume particles from North Cleft segment, Juan de Fuca Ridge. *Journal of Geophysical Research*, *99*(B3), 4985–5006. https://doi.org/10.1029/93jb02509

Findlay, A. J., Estes, E. R., Gartman, A., Yucel, M., Kamyshny, A., & Luther, G. W. (2019). Iron and sulfide nanoparticle formation and transport in nascent hydrothermal vent plumes. *Nature Communications*, *10*(1), 1597. https://doi.org/10.1038/s41467-019-09580-5

Füri, E., Hilton, D. R., Murton, B. J., Hémond, C., Dyment, J., & Day, J. M. (2011). Helium isotope variations between Réunion Island and the Central Indian Ridge (17–21 S): New evidence for ridge–hot spot interaction. *Journal of Geophysical Research*, *116*(B2), B02207. https://doi.org/10.1029/2010jb007609

Gallant, R. M., & Von Damm, K. L. (2006). Geochemical controls on hydrothermal fluids from the Kairei and Edmond vent fields, 23°–25°S, Central Indian Ridge. *Geochemistry, Geophysics, Geosystems*, *7*(6). https://doi.org/10.1029/2005GC001067

Gamo, T., Chiba, H., Yamanaka, T., Okudaira, T., Hashimoto, J., Tsuchida, S., et al. (2001). Chemical characteristics of newly discovered black smoker fluids and associated hydrothermal plumes at the Rodriguez Triple Junction, Central Indian Ridge. *Earth and Planetary Science Letters*, *193*(3–4), 371–379. https://doi.org/10.1016/S0012-821X(01)00511-8

Gamo, T., Nakayama, E., Shitashima, K., Isshiki, K., Obata, H., Okamura, K., et al. (1996). Hydrothermal plumes at the Rodriguez triple junction, Indian Ridge. *Earth and Planetary Science Letters*, *142*(1–2), 261–270. https://doi.org/10.1016/0012-821x(96)00087-8

Gamo, T., Okamura, K., Hatanaka, H., Hasumoto, H., Komatsu, D., Chinen, M., et al. (2015). Hydrothermal plumes in the Gulf of Aden, as characterized by light transmission, Mn, Fe, CH4 and δ13C-CH4 anomalies. *Deep-Sea Research Part II Topical Studies in Oceanography*, *121*, 62–70. https://doi.org/10.1016/j.dsr2.2015.06.004

Gamo, T., Tsunogai, U., Ichibayashi, S., Chiba, H., Obata, H., Oomori, T., et al. (2010). Microbial carbon isotope fractionation to produce extraordinarily heavy methane in aging hydrothermal plumes over the southwestern Okinawa Trough. *Geochemical Journal*, *44*(6), 477–487. https://doi.org/10.2343/geochemj.1.0097

Gartman, A., Findlay, A. J., & Luther, G. W., III. (2014). Nanoparticulate pyrite and other nanoparticles are a widespread component of hydrothermal vent black smoker emissions. *Chemical Geology*, *366*, 32–41. https://doi.org/10.1016/j.chemgeo.2013.12.013

German, C. R., & Seyfried, W. E. (2013). *Hydrothermal processes treatise on Geochemistry*. (Vol. 8, pp. 191–233). Elsevier Inc. https://doi.org/10.1016/B978-0-08-095975-7.00607-0

Gharib, J. J., Sansone, F. J., Resing, J. A., Baker, E. T., Lupton, J. E., & Massoth, G. J. (2005). Methane dynamics in hydrothermal plumes over a superfast spreading center: East Pacific rise, 27.5°–32.3°S. *Journal of Geophysical Research*, *110*(10), 1–16. https://doi.org/10.1029/2004JB003531

González-Santana, D., Planquette, H., Cheize, M., Whitby, H., Gourain, A., Holmes, T., et al. (2020). Processes Driving iron and Manganese dispersal from the TAG hydrothermal plume (Mid-Atlantic Ridge): Results from a GEOTRACES process study. *Frontiers in Marine Science*, *7*, 1–17. https://doi.org/10.3389/fmars.2020.00568

Graham, D. W. (2002). Noble gas isotope geochemistry of Mid-Ocean Ridge and ocean island basalts: Characterization of mantle source reservoirs. *Reviews in Mineralogy and Geochemistry*, *47*, 247–217. https://doi.org/10.1515/9781501509056-010

Haalboom, S., Price, D., Mienis, F., Witte, H., Reichart, G.-J., Duineveld, G. C., et al. (2019). Successional patterns of (trace) metals and microorganisms in the rainbow hydrothermal vent plume at the Mid-Atlantic Ridge. *Biogeosciences Discussions*, 1–44. https://doi.org/10.5194/bg-2019-189

Haymon, R. M., Fornari, D. J., Von Damm, K. L., Lilley, M. D., Perfit, M. R., Edmond, J. M., et al. (1993). Volcanic eruption of the Mid-Ocean Ridge along the East Pacific rise crest at 9°45–52′N: Direct submersible observations of seafloor phenomena associated with an eruption event in April, 1991. *Earth and Planetary Science Letters*, *119*(1–2), 85–101. https://doi.org/10.1016/0012-821X(93)90008-W

Hirota, A., Tsunogai, U., Komatsu, D. D., & Nakagawa, F. (2010). Simultaneous determination of $\delta^{15}N$ and $\delta^{18}O$ of N_2O and $\delta^{13}C$ of CH_4 in nanomolar quantities from a single water sample. *Rapid Communications in Mass Spectrometry: An International Journal Devoted to the Rapid Dissemination of Up-to-the-Minute Research in Mass Spectrometry*, *24*(7), 1085–1092. https://doi.org/10.1002/rcm.4483

Honsho, C., Tamaki, K., & Fujimoto, H. (1996). Three-dimensional magnetic and gravity studies of the Rodriguez Triple Junction in the Indian Ocean. *Journal of Geophysical Research B: Solid Earth*, *101*(7), 15837–15848. https://doi.org/10.1029/96jb00644

Ishibashi, J. I., Gamo, T., Sakai, H., Nojiri, Y., Igarashi, G., Shitashima, K., & Tsubota, H. (1988). Geochemical evidence for hydrothermal activity in the Okinawa Trough. *Geochemical Journal*, *22*(3), 107–114. https://doi.org/10.2343/geochemj.22.107

Ishibashi, J. I., Noguchi, T., Toki, T., Miyabe, S., Yamagami, S., Onishi, Y., et al. (2014). Diversity of fluid geochemistry affected by processes during fluid upwelling in active hydrothermal fields in the Izena Hole, the middle Okinawa Trough Back-Arc Basin. *Geochemical Journal*, *48*(4), 357–369. https://doi.org/10.2343/geochemj.2.0311

Ishibashi, J. I., Wakita, H., Okamura, K., Nakayama, E., Feely, R. A., Lebon, G. T., et al. (1997). Hydrothermal methane and manganese variation in the plume over the superfast-spreading southern East Pacific Rise. *Geochimica et Cosmochimica Acta*, *61*(3), 485–500. https://doi.org/10.1016/S0016-7037(96)00304-3

Jean-Baptiste, P., Bougault, H., Vangriesheim, A., Charlou, J. L., Radford-Knoery, J., Fouquet, Y., et al. (1998). Mantle 3He in hydrothermal vents and plume of the Lucky Strike site (MAR 37°17′N) and associated geothermal heat flux. *Earth and Planetary Science Letters*, *157*(1–2), 69–77. https://doi.org/10.1016/S0012-821X(98)00022-3

Jean-Baptiste, P., Charlou, J. L., Stievenard, M., Donval, J. P., Bougault, H., & Mevel, C. (1991). Helium and methane measurements in hydrothermal fluids from the mid-Atlantic ridge: The Snake Pit site at 23°N. *Earth and Planetary Science Letters*, *106*(1–4), 17–28. https://doi.org/10.1016/0012-821x(91)90060-u

Jean-Baptiste, P., Fourré, E., Charlou, J. L., German, C. R., & Radford-Knoery, J. (2004). Helium isotopes at the rainbow hydrothermal site (Mid-Atlantic Ridge, 36°14′N). *Earth and Planetary Science Letters*, *221*(1–4), 325–335. https://doi.org/10.1016/S0012-821X(04)00094-9

Jean-Baptiste, P., Mantisi, F., Pauwells, H., Grimaud, D., & Patriat, P. (1992). Hydrothermal ^{3}He and manganese plumes at 19°29′S on the Central Indian Ridge. *Geophysical Research Letters*, *19*(17), 1787–1790. https://doi.org/10.1029/92GL00577

Ji, F., Zhou, H., Yang, Q., Gao, H., Wang, H., & Lilley, M. D. (2017). Geochemistry of hydrothermal vent fluids and its implications for subsurface processes at the active Longqi hydrothermal field, Southwest Indian Ridge. *Deep-Sea Research Part I Oceanographic Research Papers*, *122*, 41–47. https://doi.org/10.1016/j.dsr.2017.02.001

Kamesh Raju, K. A., Samudrala, K., Drolia, R. K., Amarnath, D., Ramachandran, R., & Mudholkar, A. (2012). Segmentation and morphology of the Central Indian Ridge between 3°S and 11°S, Indian Ocean. *Tectonophysics*, *554–557*, 114–126. https://doi.org/10.1016/j.tecto.2012.06.001

Kawagucci, S., Miyazaki, J., Noguchi, T., Okamura, K., Shibuya, T., Watsuji, T., et al. (2016). Fluid chemistry in the Solitaire and Dodo hydrothermal fields of the Central Indian Ridge. *Geofluids*, *16*(5), 988–1005. https://doi.org/10.1111/gfl.12201

Kawagucci, S., Okamura, K., Kiyota, K., Tsunogai, U., Sano, Y., Tamaki, K., & Gamo, T. (2008). Methane, manganese, and helium-3 in newly discovered hydrothermal plumes over the Central Indian Ridge, 18°–20°S. *Geochemistry, Geophysics, Geosystems*, *9*(10). https://doi.org/10.1029/2008GC002082

Kawagucci, S., Shirai, K., Lan, T. F., Takahata, N., Tsunogai, U., Sano, Y., & Gamo, T. (2010). Gas geochemical characteristics of hydrothermal plumes at the HAKUREI and JADE vent sites, the Izena Cauldron, Okinawa Trough. *Geochemical Journal*, *44*(6), 507–518. https://doi.org/10.2343/geochemj.1.0100

Keeling, C. D. (1958). The concentration and isotopic abundances of atmospheric carbon dioxide in rural areas. *Geochimica et Cosmochimica Acta*, *13*(4), 322–334. https://doi.org/10.1016/0016-7037(58)90033-4

Keir, R. S., Schmale, O., Seifert, R., & Sültenfuß, J. (2009). Isotope fractionation and mixing in methane plumes from the Logatchev hydrothermal field. *Geochemistry, Geophysics, Geosystems*, *10*(5). https://doi.org/10.1029/2009GC002403

Kelley, D. S., Karson, J. A., Früh-Green, G. L., Yoerger, D. R., Shank, T. M., Butterfield, D. A., et al. (2005). A serpentinite-hosted ecosystem: The Lost City hydrothermal field. *Science*, *307*(5714), 1428–1434. https://doi.org/10.1126/science.1102556

Kelley, D. S., & Shank, T. M. (2010). Hydrothermal systems: A decade of discovery in slow spreading environments. *Geophysical Monograph Series*, *188*, 369–407. https://doi.org/10.1029/2010GM000945

Kim, J., Son, S. K., Kim, D., Pak, S. J., Yu, O. H., Walker, S. L., et al. (2020). Discovery of active hydrothermal vent fields along the Central Indian Ridge, 8–12 S. *Geochemistry, Geophysics, Geosystems*, *21*(8), e2020GC009058. https://doi.org/10.1029/2020gc009058

Kim, K. R. (1984). The hydrothermal vent fields in 13 °N and 11 °N on the East Pacific Rise: Alvin 1984 results. *Eos*, *65*, 973.

Kumagai, H., Nakamura, K., Toki, T., Morishita, T., Okino, K., Ishibashi, J. I., et al. (2008). Geological background of the Kairei and Edmond hydrothermal fields along the Central Indian Ridge: Implications of their vent fluids'distinct chemistry. *Geofluids*, *8*(4), 239–251. https://doi.org/10.1111/j.1468-8123.2008.00223.x

Lam, P., Cowen, J. P., & Jones, R. D. (2004). Autotrophic ammonia oxidation in a deep-sea hydrothermal plume. *FEMS Microbiology Ecology*, *47*(2), 191–206. https://doi.org/10.1016/S0168-6496(03)00256-3

Lilley, M. D., Butterfield, D. A., Olson, E. J., Lupton, J. E., MacKo, S. A., & McDuff, R. E. (1993). Anomalous CH4 and NH4+ concentrations at an unsedimented Mid-Ocean-Ridge hydrothermal system. *Nature*, *364*(6432), 45–47. https://doi.org/10.1038/364045a0

Lupton, J. (1998). Hydrothermal active seamounts introduces a ^{3}He-rich signal into the deep ocean. *Journal of Geophysical Research*, *103*(98), 853–868. https://doi.org/10.1029/98jc00146

Lupton, J. E. (1976). The ^{3}He distribution in deep water over the Mid-Atlantic Ridge. *Earth and Planetary Science Letters*, *32*(2), 371–374. https://doi.org/10.1016/0012-821X(76)90077-7

Lupton, J. E. (1995). *Hydrothermal plumes: Near and far field* (Vol. 91, pp. 317–346). Washington DC American Geophysical Union Geophysical Monograph Series.

Merlivat, L., Pineau, F., & Javoy, M. (1987). Hydrothermal vent waters at 13°N on the east Pacific Rise: Isotopic composition and gas concentration. *Earth and Planetary Science Letters*, *84*(1), 100–108. https://doi.org/10.1016/0012-821X(87)90180-4

Morishita, T., Hara, K., Nakamura, K., Sawaguchi, T., Tamura, A., Arai, S., et al. (2009). Igneous, alteration and exhumation processes recorded in abyssal peridotites and related fault rocks from an oceanic core complex along the Central Indian Ridge. *Journal of Petrology*, *50*(7), 1299–1325. https://doi.org/10.1093/petrology/egp025

Morishita, T., Nakamura, K., Shibuya, T., Kumagai, H., Sato, T., Okino, K., et al. (2015). Petrology of peridotites and related gabbroic rocks around the Kairei hydrothermal field in the Central Indian Ridge. In *Subseafloor biosphere linked to hydrothermal systems* (pp. 177–193). Springer. https://doi.org/10.1007/978-4-431-54865-2_14

Mottl, M. J., & McConachy, T. F. (1990). Chemical processes in buoyant hydrothermal plumes on the East Pacific Rise near 21°N. *Geochimica et Cosmochimica Acta*, *54*(7), 1911–1927. https://doi.org/10.1016/0016-7037(90)90261-I

Mottl, M. J., Sansone, F. J., Geoffrey Wheat, C., Resing, J. A., Baker, E. T., & Lupton, J. E. (1995). Manganese and methane in hydrothermal plumes along the East Pacific Rise, 8°40′ to 11°50′N. *Geochimica et Cosmochimica Acta*, *59*(20), 4147–4165. https://doi.org/10.1016/0016-7037(95)00245-U

Nakamura, K., Morishita, T., Bach, W., Klein, F., Hara, K., Okino, K., et al. (2009). Serpentinized troctolites exposed near the Kairei Hydrothermal Field, Central Indian Ridge: Insights into the origin of the Kairei hydrothermal fluid supporting a unique microbial ecosystem. *Earth and Planetary Science Letters*, *280*(1–4), 128–136. https://doi.org/10.1016/j.epsl.2009.01.024

Nakamura, K., Watanabe, H., Miyazaki, J., Takai, K., Kawagucci, S., Noguchi, T., et al. (2012). Discovery of new hydrothermal activity and chemosynthetic fauna on the Central Indian ridge at 18°–20°S. *PLoS One*, *7*(3), e32965. https://doi.org/10.1371/journal.pone.0032965

Okino, K., Nakamura, K., & Sato, H. (2015). Tectonic background of four hydrothermal fields along the Central Indian Ridge. In *Subseafloor biosphere linked to hydrothermal systems: TAIGA concept* (pp. 133–146). https://doi.org/10.1007/978-4-431-54865-2_11

Ortega-Osorio, A., & Scott, S. D. (2001). Morphological and chemical characterization of neutrally buoyant plume-derived particles at the eastern Manus Basin hydrothermal field, Papua New Guinea. *The Canadian Mineralogist*, *39*(1), 17–31. https://doi.org/10.2113/gscanmin.39.1.17

Ray, D., Babu, E. V. S. S. K., & Prakash, L. S. (2017). Nature of suspended particles in hydrothermal plume at 3°40'N Carlsberg Ridge: A comparison with deep oceanic suspended matter. *Current Science*, *112*(1), 139–146. https://doi.org/10.18520/cs/v112/i01/139-146

Ray, D., Kamesh Raju, K. A., Baker, E. T., Srinivas Rao, A., Mudholkar, A. V., Lupton, J. E., et al. (2012). Hydrothermal plumes over the Carlsberg Ridge, Indian Ocean. *Geochemistry, Geophysics, Geosystems*, *13*(1), Q01009. https://doi.org/10.1029/2011GC003888

Ray, D., Kamesh Raju, K. A., Srinivas Rao, A., SuryaPrakash, L., Mudholkar, A. V., Yatheesh, V., et al. (2020). Elevated turbidity and dissolved manganese in deep water column near 10°47'S Central Indian Ridge: Studies on hydrothermal activities. *Geo-Marine Letters*, *40*(5), 619–628. https://doi.org/10.1007/s00367-020-00657-5

Ray, D., Mirza, I. H., Surya Prakash, L., Kaisary, S., Sarma, Y. V. B., Rao, B. R., et al. (2008). Water-column geochemical anomalies associated with the remnants of a mega plume: A case study after CR-2003 hydrothermal event in Carlsberg Ridge, NW Indian Ocean. *Current Science*, *95*(3), 355–360.

Resing, J. A., Baker, E. T., Lupton, J. E., Walker, S. L., Butterfield, D. A., Massoth, G. J., & Nakamura, K. I. (2009). Chemistry of hydrothermal plumes above submarine volcanoes of the Mariana Arc. *Geochemistry, Geophysics, Geosystems*, *10*(2). https://doi.org/10.1029/2008GC002141

Resing, J. A., & Mottl, M. J. (1992). Determination of Manganese in seawater using flow injection analysis with On-line Preconcentration and spectrophotometric detection. *Analytical Chemistry*, *64*(22), 2682–2687. https://doi.org/10.1021/ac00046a006

Rudnicki, M. D., & Elderfield, H. (1992). Helium, radon and manganese at the TAG and Snakepit hydrothermal vent fields, 26° and 23°N, Mid-Atlantic Ridge. *Earth and Planetary Science Letters*, *113*(3), 307–321. https://doi.org/10.1016/0012-821x(92)90136-j

Ryu, T., Woo, S., & Lee, N. (2019). The first reference transcriptome assembly of the stalked barnacle, Neolepas Marisindica, from the Onnuri Vent Field on the Central Indian Ridge. *Marine Genomics*, *48*, 100679. https://doi.org/10.1016/j.margen.2019.04.004

Sakai, H., Gamo, T., Kim, E.-S., Shitashima, K., Yanagisawa, F., Tsutsumi, M., et al. (1990). Unique chemistry of the hydrothermal solution in the Mid-Okinawa Trough Backarc Basin. *Geophysical Research Letters*, *17*(12), 2133–2136. https://doi.org/10.1029/GL017i012p02133

Sansone, F. J., Holmes, M. E., & Popp, B. N. (1999). Methane stable isotopic ratios and concentrations as indicators of methane dynamics in estuaries. *Global Biogeochemical Cycles*, *13*(2), 463–474. https://doi.org/10.1029/1999GB900012

Sato, H., Nakamura, K., Kumagai, H., Senda, R., Morishita, T., Tamura, A., & Arai, S. (2015). Petrology and geochemistry of Mid-Ocean Ridge Basalts from the southern central Indian Ridge. In *Subseafloor biosphere linked to hydrothermal systems: TAIGA concept* (pp. 163–175). https://doi.org/10.1007/978-4-431-54865-2_13

Sato, T., Okino, K., & Kumagai, H. (2009). Magnetic structure of an oceanic core complex at the southernmost Central Indian Ridge: Analysis of shipboard and deep-sea three-component magnetometer data. *Geochemistry, Geophysics, Geosystems*, *10*(6). https://doi.org/10.1029/2008GC002267

Schmid, F., Peters, M., Walter, M., Devey, C., Petersen, S., Yeo, I., et al. (2019). Physico-chemical properties of newly discovered hydrothermal plumes above the Southern Mid-Atlantic Ridge (13°–33°S). *Deep-Sea Research Part I Oceanographic Research Papers*, *148*, 34–52. https://doi.org/10.1016/j.dsr.2019.04.010

Schmidt, K., Koschinsky, A., Garbe-Schönberg, D., de Carvalho, L. M., & Seifert, R. (2007). Geochemistry of hydrothermal fluids from the ultramafic-hosted Logatchev hydrothermal field, 15°N on the Mid-Atlantic Ridge: Temporal and spatial investigation. *Chemical Geology*, *242*(1–2), 1–21. https://doi.org/10.1016/j.chemgeo.2007.01.023

Son, J., Pak, S. J., Kim, J., Baker, E. T., You, O. R., Son, S. K., & Moon, J. W. (2014). Tectonic and magmatic control of hydrothermal activity along the slow-spreading Central Indian Ridge, 8S–17S. *Geochemistry, Geophysics, Geosystems*, *15*(5), 2011–2020. https://doi.org/10.1002/2013GC005206

Srinivas Rao, A., & Kurian, J. P. (2018). Mapping of two new hydrothermal plumes in southern Central Indian Ridge, Indian Ocean. *SCOR-IR workshop abstract volume, S1-PS-02*, 10.

Stüben, D., Stoffers, P., Cheminée, J. L., Hartmann, M., McMurtry, G. M., Richnow, H. H., et al. (1992). Manganese, methane, iron, zinc, and nickel anomalies in hydrothermal plumes from Teahitia and MacDonald volcanoes. *Geochimica et Cosmochimica Acta*, *56*(10), 3693–3704. https://doi.org/10.1016/0016-7037(92)90162-C

Takahata, N., Shirai, K., Ohmori, K., Obata, H., Gamo, T., & Sano, Y. (2018). Distribution of helium-3 plumes and deep-sea circulation in the central Indian Ocean. *Terrestrial, Atmospheric and Oceanic Sciences*, *29*(3), 331–340. https://doi.org/10.3319/TAO.2017.10.21.02

Takai, K., Gamo, T., Tsunogai, U., Nakayama, N., Hirayama, H., Nealson, K. H., & Horikoshi, K. (2004). Geochemical and microbiological evidence for a hydrogen-based, hyperthermophilic subsurface lithoautotrophic microbial ecosystem (HyperSLiME) beneath an active deep-sea hydrothermal field. *Extremophiles*, *8*(4), 269–282. https://doi.org/10.1007/s00792-004-0386-3

Tao, C., Seyfried, W. E., Lowell, R. P., Liu, Y., Liang, J., Guo, Z., et al. (2020). Deep high-temperature hydrothermal circulation in a detachment faulting system on the ultra-slow spreading ridge. *Nature Communications*, *11*(1), 1300. https://doi.org/10.1038/s41467-020-15062-w

Tsunogai, U., Ishibashi, J., Wakita, H., & Gamo, T. (1998). Methane-rich plumes in the Suruga Trough (Japan) and their carbon isotopic characterization. *Earth and Planetary Science Letters*, *160*(1–2), 97–105. https://doi.org/10.1016/s0012-821x(98)00075-2

Tsunogai, U., Miyoshi, Y., Matsushita, T., Komatsu, D. D., Ito, M., Sukigara, C., & Maruo, M. (2020). Dual stable isotope characterization of excess methane in oxic waters of a Mesotrophic Lake. *Limnology & Oceanography*, *65*(12), 2937–2952. https://doi.org/10.1002/lno.11566

Tsunogai, U., Yoshida, N., Ishibashi, J., & Gamo, T. (2000). Carbon isotopic distribution of methane in deep-sea hydrothermal plume, Myojin Knoll Caldera, Izu-Bonin Arc: Implications for microbial methane oxidation in the oceans and applications to heat flux estimation. *Geochimica et Cosmochimica Acta*, *64*(14), 2439–2452. https://doi.org/10.1016/S0016-7037(00)00374-4

Van Dover, C. L., Humphris, S. E., Fornari, D., Cavanaugh, C. M., Collier, R., Goffredi, S. K., et al. (2001). Biogeography and ecological setting of Indian Ocean hydrothermal vents. *Science*, *294*(5543), 818–823. https://doi.org/10.1126/science.1064574

Von Damm, K. L., Bray, A. M., Buttermore, L. G., & Oosting, S. E. (1998). The geochemical controls on vent fluids from the Lucky Strike vent field, Mid-Atlantic Ridge. *Earth and Planetary Science Letters*, *160*(3–4), 521–536. https://doi.org/10.1016/S0012-821X(98)00108-3

Von Damm, K. L., Edmond, J. M., Grant, B., Measures, C. I., Walden, B., & Weiss, R. F. (1985). Chemistry of submarine hydrothermal solutions at 21 °N, East Pacific Rise. *Geochimica et Cosmochimica Acta*, *49*(11), 2197–2220. https://doi.org/10.1016/0016-7037(85)90222-4

Wang, H., Yang, Q., Ji, F., Lilley, M. D., & Zhou, H. (2012). The geochemical characteristics and Fe(II) oxidation kinetics of hydrothermal plumes at the Southwest Indian Ridge. *Marine Chemistry*, *134–135*, 29–35. https://doi.org/10.1016/j.marchem.2012.02.009

Welhan, J. A., & Craig, H. (1983). Methane, hydrogen and helium in hydrothermal fluids at 21°N on the East Pacific Rise. In *Hydrothermal processes at seafloor spreading centers* (pp. 391–409). https://doi.org/10.1007/978-1-4899-0402-7_17

Whiticar, M. J. (1999). Carbon and hydrogen isotope systematics of bacterial formation and oxidation of methane. *Chemical Geology*, *161*(1), 291–314. https://doi.org/10.1016/S0009-2541(99)00092-3

Yi, S. B., Oh, C. W., Pak, S. J., Kim, J., & Moon, J. W. (2014). Geochemistry and petrogenesis of mafic-ultramafic rocks from the Central Indian Ridge, latitude 8°–17°S: Denudation of mantle harzburgites and gabbroic rocks and compositional variation of basalts. *International Geology Review*, *56*(14), 1691–1719. https://doi.org/10.1080/00206814.2014.955539

You, O. R., Son, S. K., Baker, E. T., Son, J., Kim, M. J., Barcelona, M. J., & Kim, M. (2014). Bathymetric influence on dissolved methane in hydrothermal plumes revealed by concentration and stable carbon isotope measurements at newly discovered venting sites on the Central Indian Ridge (11–13°S). *Deep-Sea Research Part I Oceanographic Research Papers*, *91*, 17–26. https://doi.org/10.1016/j.dsr.2014.05.011

Yücel, M., Gartman, A., Chan, C. S., & Luther, G. W. (2011). Hydrothermal vents as a kinetically stable source of iron-sulphide-bearing nanoparticles to the ocean. *Nature Geoscience*, *4*(6), 367–371. https://doi.org/10.1038/ngeo1148

Yue, X., Li, H., Ren, J., Tao, C., Zhou, J., Wang, Y., & Lü, X. (2019). Seafloor hydrothermal activity along Mid-Ocean Ridge with strong melt supply: Study from segment 27, southwest Indian ridge. *Scientific Reports*, *9*(1), 9874. https://doi.org/10.1038/s41598-019-46299-1

Zhu, J., Lin, J., Guo, S., & Chen, Y. (2008). Hydrothermal plume anomalies along the Central Indian Ridge. *Chinese Science Bulletin*, *53*(16), 2527–2535. https://doi.org/10.1007/s11434-008-0208-6